# Proline oxidation leading to high electron flow through reduction of ubiquinone supports ATP production by $F_1F_0$-ATPase in mitochondria with inhibited Complex I

Gergely Pallag[1], Sara Nazarian[1], Dora Ravasz[1], David Bui[1], Timea Komlódi[2], Carolina Doerrier[2], Erich Gnaiger[2], Thomas N Seyfried[3], Christos Chinopoulos[1*]

[1] Department of Biochemistry and Molecular Biology, Semmelweis University, Budapest 1094, Hungary
[2] Oroboros Instruments, Innsbruck, Austria
[3] Biology Department, Boston College, Chestnut Hill, MA 02467, USA

* Corresponding author:
chinopoulos.christos@eok.sote.hu

## Abstract

**In mitochondria expressing proline dehydrogenase (ProDH), oxidation of proline to pyrroline-5-carboxylate (P5C) leads to transfer of electrons to ubiquinone supporting Complexes CIII and CIV, in turn generating the protonmotive force. Further catabolism of P5C forms glutamate that fuels the citric acid cycle yielding reducing equivalents sustaining oxidative phosphorylation. However, P5C and glutamate catabolism depend on CI activity due to NAD⁺ requirement. The extent of proline oxidation was established in isolated mitochondria of various mouse tissues by means of simultaneously measuring oxygen consumption, membrane potential, NADH and ubiquinone redox state using the NextGen-O2k (Oroboros Instruments) and correlated to ProDH activity and F1F0-ATPase directionality. In CI-inhibited mouse liver and kidney mitochondria exhibiting high levels of proline oxidation and ProDH**

activity, catabolism of proline generated a sufficiently high membrane potential maintaining $F_1F_0$-ATPase operation in forward mode. This was not observed when either CIII or CIV was inhibited, nor during anoxia. Fueling CIII and CIV with duroquinone partially reproduced the effects of proline. Excess glutamate could not reproduce the effects of proline, arguing that they are due to processes upstream of glutamate conversion from proline. The ProDH inhibitors L-tetrahydro-2-furoic acid and to lesser extent S-5-oxo-2-tetrahydrofurancarboxylic acid abolished all effects conferred by proline. It is concluded that proline catabolism through ProDH generates sufficient CIII and CIV proton pumping, supporting ATP production by $F_1F_0$-ATPase even when CI is inhibited.

# 1. Introduction

Proline oxidation has been discovered in mitochondria isolated from rabbit kidneys by Taggart and Krakaur in 1949 [1]. In 1962, Johnson and Strecker reproduced this in rat liver mitochondria [2] and in 1986 McKnight and Hird demonstrated proline oxidation in mitochondria from other rat tissues [3]. Although proline oxidation has received most attention in insect flight muscle [4], [5], [6], pioneering studies by Phang and co-workers have established a specialized role for this amino acid in cancer metabolism [7], [8].

Hereby, we investigated the effect of proline oxidation in providing sufficient bioenergetic drive in supporting mitochondrial ATP production when respiratory Complex CI was inhibited. Mindful that proline catabolism exhibits strong tissue-dependence, we measured the extent of proline oxidation in isolated mitochondria obtained from various mouse tissues; to the best of our knowledge, proline catabolism (and in particular ProDH activity) has been investigated in mouse only in liver mitochondria [9]. We report that only in tissues with high ProDH activity, proline could maintain ATP formation by the mitochondrial $F_1F_0$-ATPase when CI was inhibited by rotenone. This effect was mediated by reduction of ubiquinone (UQ) fueling Complexes CIII and CIV in turn generating membrane potential, and not due to oxidation of glutamate which is formed by catabolism of proline. Our results argue that proline catabolism can completely bypass CI blockade avoiding a bioenergetic collapse.

# 2. Results

## 2.1. Overview of proline metabolism in mitochondria

The metabolism of proline in mitochondria is briefly outlined in Figure 1; for a more detailed review see [10] and [11]. As shown in Figure 1, proline enters mitochondria through a bidirectional transporter. Unlike for the plasma membrane in which twelve transporters have been identified and characterized [12], transport of proline across the

mitochondrial inner membrane has been regarded only as "energy-dependent" [13] and mediated by two entities: a proline uniporter and proline/glutamate antiporter [14]; the genetic identities of these transporters are still unknown. The rate of proline transport by these two mitochondrial transporters is similar to the first two steps of proline oxidation, indicating that transport is not a limiting factor of proline metabolism [13]. Once inside the matrix, proline is irreversibly converted to pyrroline-5-carboxylate (P5C) by proline dehydrogenase/proline oxidase (ProDH). There are two ProDH enzymes; ProDH1, converting L-proline to P5C and ProDH2 which catalyzes the conversion of hydroxyproline to pyrroline-3-hydroxy-5-carboxylate [15]. ProDH2 can also use proline as a substrate but with a much lower efficiency [15]. ProDH enzymes are FAD-bound, reducing UQ [9], [16]. The requirement of ubiquinone in proline oxidation has been reported by Erecińska in 1965 [17]. Reduced Q (ubiquinol, $UQH_2$) fuels CIII, subsequently transferring electrons to CIV, provided that a suitable final electron acceptor is available [9]. P5C tautomerizes non-enzymatically to glutamate semi-aldehyde (GSA). GSA may have two fates: i) transamination with glutamate to ornithine and oxoglutarate (Og; α-ketoglutarate) by ornithine aminotransferase (OAT), and/or ii) oxidation to glutamate by delta-1-pyrroline-5-carboxylate dehydrogenase (ALDH4A1) concomitantly reducing $NAD(P^+)$ to NAD(P)H. Glutamate may then enter the citric acid cycle either through glutamate dehydrogenase yielding oxoglutarate, or through transamination with oxaloacetate to oxoglutarate and aspartate by aspartate aminotransferase (ASAT).

Mindful of the above metabolic considerations, we investigated the effects of adding proline to mitochondria by measuring i) oxygen consumption (final electron acceptor of CIV that receives electrons from CIII fueled by $UQH_2$ generated by ProDH), ii) $NAD^+$ reduction reflecting ALDH4A1, GDH and citric acid cycle dehydrogenases activities, iii) ubiquinone reduction by ProDH while converting proline to P5C, iv) generation of mitochondrial membrane potential ($\Delta\Psi_{mt}$) by CIII and CIV proton pump activity and subsequent use of these protons by $F_1F_0$-ATPase and downstream events altering matrix ATP/ADP (in the presence of CI inhibition), and v) the directionalities of $F_1F_0$-ATPase and the adenine nucleotide translocase (ANT) which are profoundly influenced by the ATP/ADP ratio, [18], [18], also in the presence of CI inhibition. Data obtained from these experiments were correlated with ProDH activity values estimated from the same tissues.

## 2.2. Kinetic characterization of proline dehydrogenase in mitochondria isolated from various mouse tissues

To the best of our knowledge, ProDH activity in murine tissues has been reported only from mouse liver [9] and various organs of the rat [3]. Thus, we first measured ProDH catalytic activity content in isolated mitochondria from mouse liver, kidney, brain and heart, and also determined the apparent $K_m$ of mouse liver ProDH for proline. As shown in Figure 2A, liver and kidney mitochondria exhibited much higher ProDH activity than brain and heart mitochondria, as similarly reported for rat tissues in [3]. We further determined the apparent $K_m$ of ProDH for proline in mouse liver mitochondria and report it to be 3.08 ± 0.48 mM (Figure 2B), estimated by non-linear fitting. Values of 2.4 mM for fetal and adult rat liver mitochondria [19] and 0.42-1.2 mM in DLD-POX cells [9] have been previously reported.
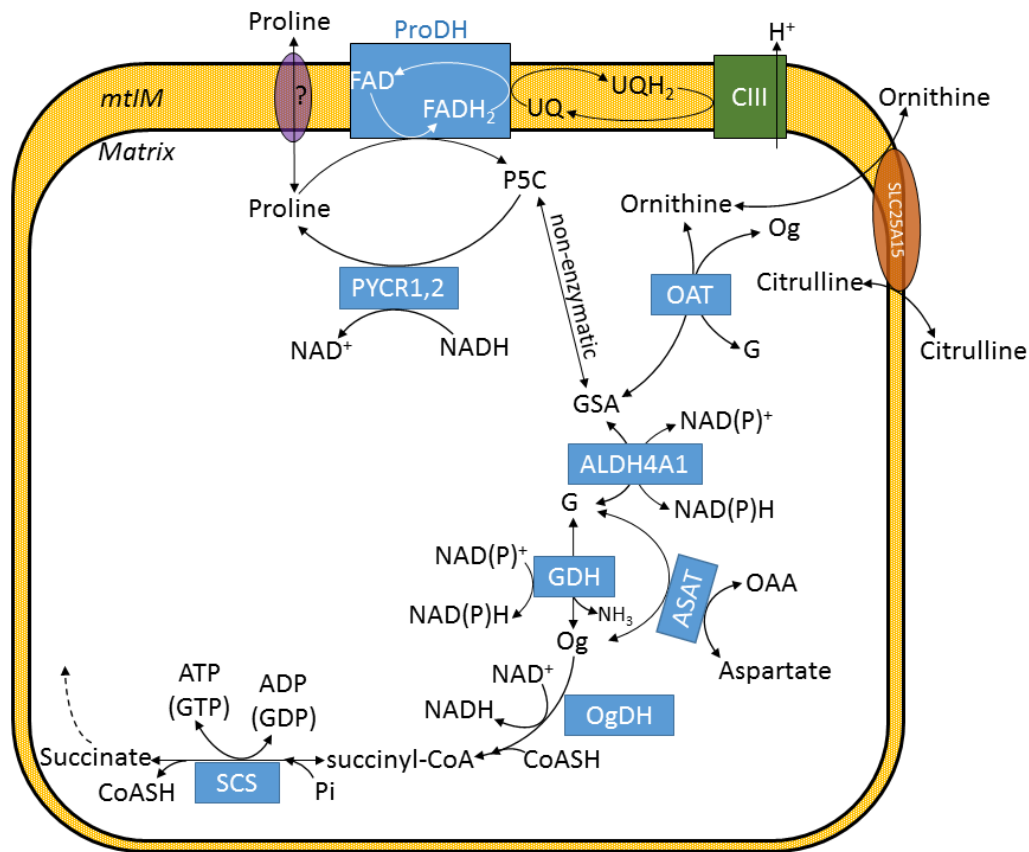
**Figure 1. The pathway of proline metabolism**. Og: oxoglutarate; ALDH4A1: Aldehyde Dehydrogenase 4 Family Member A1 (L-Glutamate Gamma-Semialdehyde Dehydrogenase); ASAT: aspartate aminotransferase; CIII: Complex III; G: glutamate; GDH: glutamate dehydrogenase; GSA: glutamate semi-aldehyde; mtIM: mitochondrial inner membrane; OAA: oxaloacetate; OAT: ornithine aminotransferase; OgDH: oxoglutarate dehydrogenase; P5C: pyrroline-5-carboxylate; ProDH: proline dehydrogenase; PYCR1,2: pyrroline-5-carboxylate reductase isoforms 1 or 2; SLC25A15: solute carrier family 25 member 15; SCS: succinate-CoA ligase (succinyl-CoA synthetase).

## 2.3. Liver and kidney mitochondria respire on proline

Having measured the tissue-dependent ProDH activity in isolated mitochondria from mouse tissues, we sought to establish the extent of proline catabolism as a respiratory substrate. The effect of proline on oxygen consumption rates (and all subsequent experiments) was tested in the 0.25-10 mM concentration range. This is because the normal human plasma concentration of this amino acid is in the range of 100–250 µM [20], , [21], [22], [23], [13]. However, in patients suffering from type 2 diabetes, obesity, insulin resistance [24], or cancer-associated cachexia [25], an almost two-fold increase has been reported. Similar to humans, plasma proline concentration in the range of 0.25-0.3 mM has been observed in the rat [26].

**Figure 2. Kinetic characterization of ProDH activity in isolated mitochondria**. **(A)** ProDH catalytic activity content (expressed in pkat/mg) of mitochondria isolated from mouse liver, kidney, brain and heart, using sat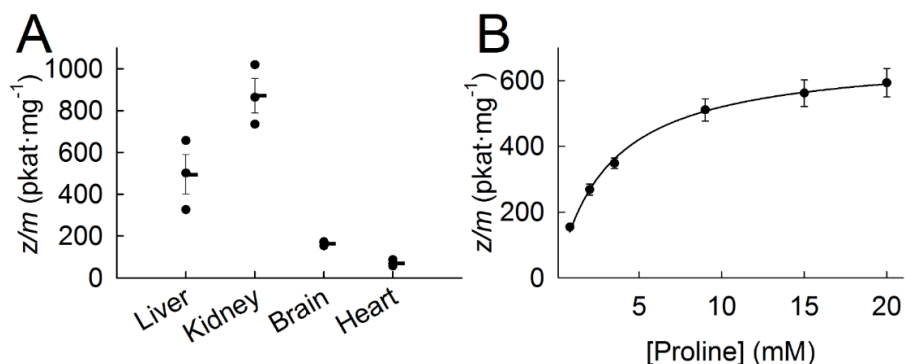urating concentration of proline (100 mM). Data are SEM averaged from 3 independent experiments. **(B)** Determination of apparent $K_m$ of mouse liver ProDH for proline. Data points are SEM averaged from 3 independent experiments.

**Table 1. Additivity of convergent succinate and proline pathway OXPHOS capacity in liver and kidney mitochondria**. Median additivity >1 indicates 'excess additivity' and synergistic activation of $O_2$ flux, when flux of the combined pathway $J_{SPro}$ is higher than the arithmetic sum of fluxes for the individual pathways $J_{Pro}+J_S$. Negative additivity indicates suppression of flux in the presence of the substrate combination [29].

| | Proline [mM] | Succinate [mM] | $J_{Pro}/J_{SPro}$ | $J_S/J_{SPro}$ | Additivity |
|---|---|---|---|---|---|
| Liver OXPHOS | 2 | 5 | 0.30 | 0.40 | 2.04 |
| | 5 | 5 | 0.30 | 0.41 | 1.95 |
| Liver LEAK | 2 | 5 | 0.55 | 0.67 | 0.59 |
| | 5 | 5 | 0.40 | 0.59 | 1.03 |
| Kidney OXPHOS | 2 | 5 | 0.19 | 0.60 | 2.11 |
| | 5 | 5 | 0.26 | 0.58 | 1.62 |
| Kidney LEAK | 2 | 5 | 0.25 | 1.10 | -0.39 |
| | 5 | 5 | 0.39 | 1.08 | -0.20 |

As shown in Figure 3A for liver and 3F for kidney, proline led to a dose-dependent (0.25-10 mM) increase in LEAK and OXPHOS respiration (kinetically saturating ADP [27]) of isolated mitochondria. The proline-induced increases in LEAK and OXPHOS respiration were, however, masked if glutamate & malate (Figure 3B for liver and 3G in kidney) or glutamate & malate & β-hydroxybutyrate (βOH, Figure 3C in liver) or glutamate & malate & itaconate (Figure 3H in kidney) were present. βOH increases the NADH/NAD+ ratio due to the high activity of β-hydroxybutyrate dehydrogenase in the liver, while itaconate (Itac) limits mitochondrial substrate-level phosphorylation as it is a preferred substrate for succinate-CoA ligase also leading to a CoASH-trap [28], thus exerting metabolic pressure on the overall citric acid cycle. The increases in OXPHOS capacitys were not merely additive but strongly synergistic to that conferred by succinate in liver (Figures 3D and 3E) and kidney mitochondria (Figures 3I and 3J). OXPHOS capacity with the

succinate & proline substrate combination ($J_{SPro}$) was 1.4- and 1.2-fold higher than the arithmetic sum $J_{Pro} + J_S$ (Table 1), demonstrating a synergistic effect and excess additivity [29]. In contrast, additivity in the LEAK state was partially or completely additive in liver mitochondria. In kidney mitochondria, additivity was even negative in the LEAK state, indicating suppression of LEAK respiration when proline was added to succinate (Table 1; Supplement Table S1).

## 2.4. Effect of proline on ΔΨmt, NADH autofluorescence and Q redox state of isolated mitochondria

Mindful that in the presence of NADH-linked substrates (glutamate, malate, βOH) addition of proline did not yield an additional increase in oxygen consumption rate, we questioned whether this was because of downstream production of glutamate (see Figure 1) fueling the citric acid cycle or a limitation of the measurement itself, having saturated the capacity of CIV transferring electrons to molecular oxygen. Therefore, we examined the effects of proline on other bioenergetic readouts, namely ΔΨmt, NADH autofluorescence and Q redox state of isolated mitochondria. As shown in Figure 4A for liver and 6A for kidney, mitochondria were added in the buffer without substrates and allowed to develop a transient membrane potential before exhibiting depletion of endogenous substrates, leading to a complete loss of ΔΨmt. Subsequently, proline was added in boluses at the concentrations indicated in the panels, leading to a progressive polarization. Further addition of glutamate (G) and malate (M) did not yield any further increase in ΔΨmt. On the other hand, addition of succinate (S; Figures 4B for liver and 6B for kidney mitochondria) led to a further decrease in safranine O fluorescence indicative of a gain in ΔΨmt even in the presence of rotenone. Importantly, the presence of rotenone did not abolish the proline-induced polarization. However, the CIII inhibitor, myxothiazol, completely inhibited the proline-induced polarization in both liver (Figure 4D) and kidney (Figure 6C) mitochondria. On the other hand, atpenin A5 blocked the succinate-induced gain in ΔΨmt but the proline-induced changes remained unaffected (Figure 4C for liver mitochondria).

In congruence to the data showing ΔΨmt, additions of proline to mitochondria led to a dose-dependence increase in NADH autofluorescence; NADH autofluorescence was recorded fluorometrically using two different equipment: a Hitachi F-7000 fluorescence spectrophotometer, or an Oroboros NextGen-O2k. Data obtained with the Hitachi are shown in Figure 4E (for liver mitochondria) and 6D (for kidney mitochondria), while those obtained with the NextGen-O2k are shown in Figure 4G (for liver mitochondria) and 8B (for kidney mitochondria). Oxygen consumption rate, NADH autofluorescence and rhodamine 123 fluorescence (indicative of ΔΨmt) were simultaneously recorded and shown in Figure panels 4F, G and H, respectively for liver and 8A, B, and C for kidney, aligned on the dashed grey lines, using the NextGen-O2k. As shown in Figures 4E, 4G, 6D, and 8B subsequent addition of rotenone led to greater increases in NADH autofluorescence depending on the amount of proline added to mitochondria. This additional increase in NADH depending on proline concentration reflects the NADH originating from the reaction catalyzed by ALDH4A1 which is upstream to glutamate (see Figure 1).
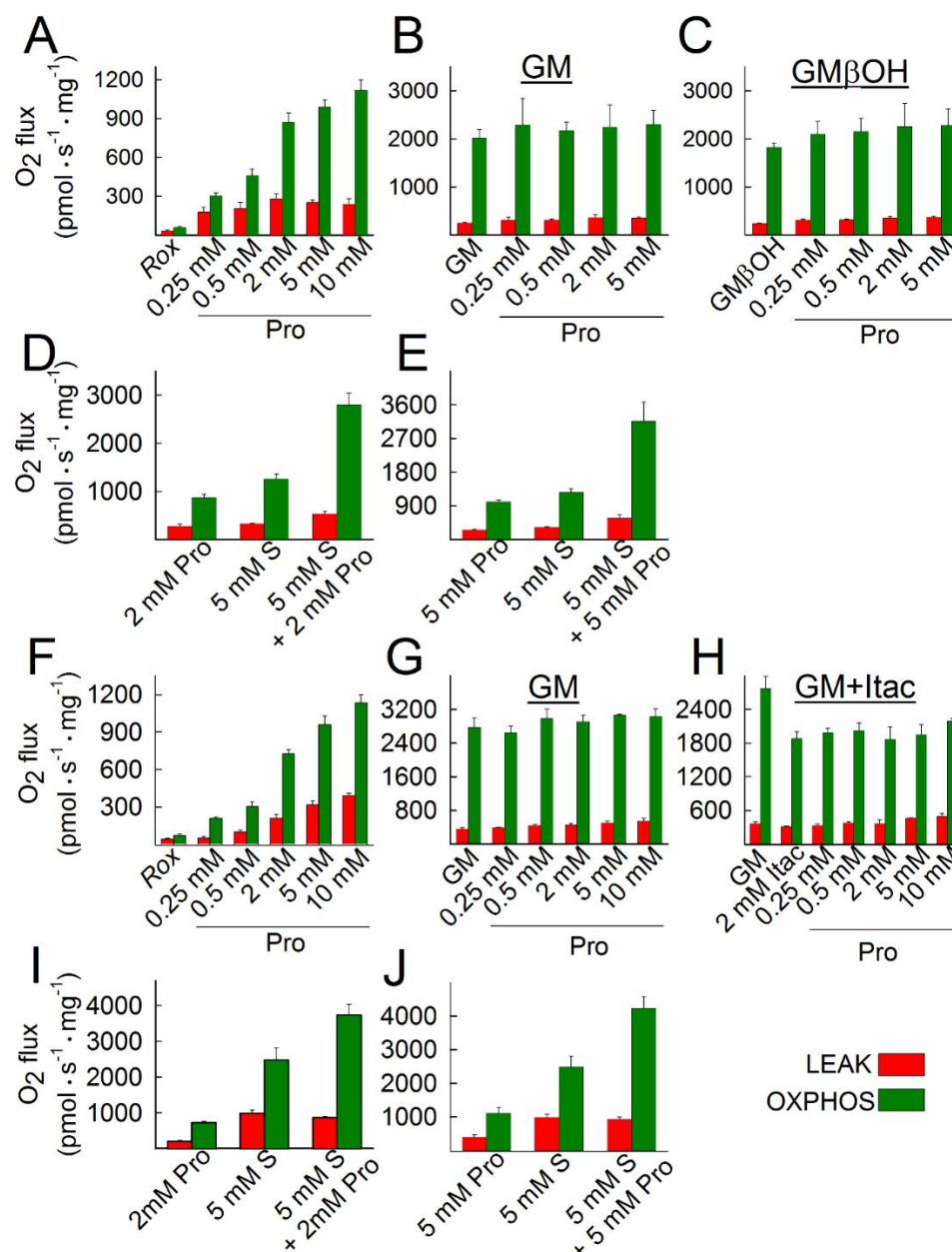
**Figure 3. The effect of proline concentration on oxygen consumption rates (LEAK: red bars; OXPHOS: green bars) of isolated mouse liver mitochondria (A-E) and mouse kidney (F-J) mitochondria using various substrate combinations and concentrations**. **(A, F)** *Rox*: residual oxygen consumption (no external substrate added; increased OXPHOS indicates the effect of ADP stimulating respiration on internal substrates), followed by proline titrations. **(B, G)** GM: glutamate&malate, followed by proline titrations. **(C)** GM & 2 mM βOH, followed by proline titration . **(H)** GM: glutamate&malate, 2 mM Itac: GM+2 mM itaconate, followed by proline titration. Proline (Pro) **(D, I)** and/or succinate (S) **(E, J)**. Data are SEM averaged from at least 3 independent experiments.

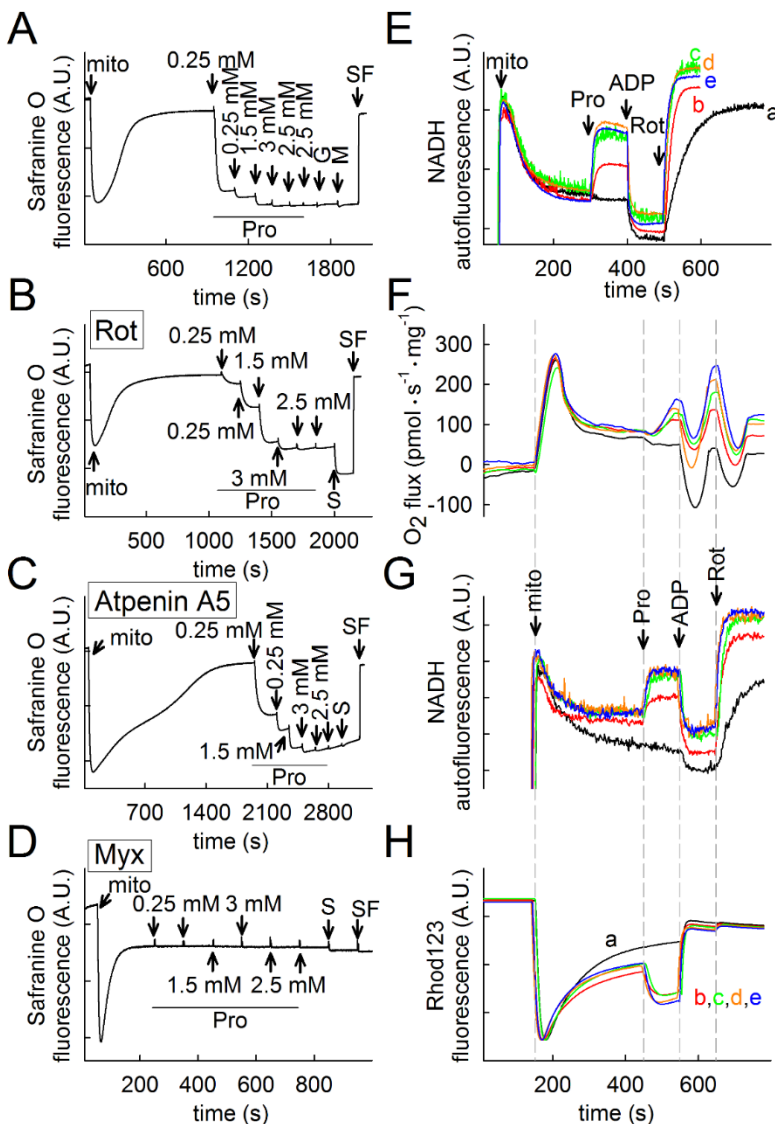**Figure 4. Effect of proline concentration on $\Delta\Psi_{mt}$ and NADH autofluorescence of isolated mouse liver mitochondria subjected to targeted inhibition of electron transfer (ET) pathways**. No substrates present prior to addition of mitochondria. Glutamate (G), malate (M), and proline (Pro) added at concentrations indicated. **(A-D)** Time course of safranine O signal indicative of $\Delta\Psi_{mt}$ (arbitrary units, A.U.). SF6847 (SF, 1 µM). **(A)** No targeted inhibition of electron transfer pathways. **(B)** 1 µM rotenone (Rot) present in the buffer prior to addition of mitochondria; succinate (S, 5 mM). **(C)** As in B, but 1 µM atpenin A5 replaced Rot. **(D)** As in B, but myxothiazol (Myx) replaced Rot. **(E-H)** Concentrations of Pro: black (a): 0 mM, red (b): 0.25 mM, green (c): 0.5 mM, orange (d): 2 mM, blue (e): 5 mM. **(E)** NADH autofluorescence (arbitrary units A.U.) measured in the Hitachi F-7000 fluorescence spectrophotometer. **(F-H)** Oxygen consumption, NADH autofluorescence, and rhodamine 123 fluorescence indicative of $\Delta\Psi_{mt}$ (arbitrary units A.U.), respectively, recorded simultaneously from the same liver mitochondria using the NextGen-O2k and aligned on the dashed grey lines.

To strengthen the above conclusions that proline is catabolized in liver and kidney mitochondria, we recorded quinone (Q) redox state using an Oroboros NextGen-O2k, simultaneous to oxygen consumption rate and rhodamine 123 fluorescence (indicative of $\Delta\Psi_{mt}$). As shown in Figure panels 5A, B, C (for liver mitochondria) and 7A, B, C (for kidney mitochondria) bolus additions of proline (concentrations indicated in the panels) led to measurable increases in oxygen consumption rates, Q reduction and gains in $\Delta\Psi_{mt}$. The increases in Q reduction were less pronounced in the presence of rotenone (Figure panels

5E for liver and 7E for kidney mitochondria) than in the absence of this CI inhibitor (panels 5B and 7B, for liver and kidney mitochondria, respectively). The changes in Q reduction are shown as a non-calibrated signal; thus, at the end of the experiments, succinate was added followed by SF6847. This was done in order to provide a semi-quantitative estimation of Q reduction by proline compared to reduction by succinate dehydrogenase and oxidation of ETS due to the uncoupler. As expected, in the presence of CIII inhibitor, myxothiazol, proline led to no changes in Q reduction state (Figure 5H), monitored simultaneously to oxygen consumption rate (Figure 5G) and rhodamine 123 fluorescence (Figure 5I).



**Figure 5. Coenzyme Q (Q) redox state recorded simultaneously with oxygen consumption rate and rhodamine 123 fluorescence in isolated mouse liver mitochondria using the NextGen-O2k. (A)** Oxygen consumption. **(B)** Q redox state. **(C)** Rhodamine 123 fluorescence indicative of $\Delta\Psi_{mt}$ (arbitrary units A.U.). No substrates were present. Succinate (S, 5 mM), Proline (Pro) added at the concentrations indicated. **(D-F)** As in A, B, and C, but rotenone was present in the medium. 0.25 μM SF. **(G-I)** As in A, B, and C, but 0.1 μM myxothiazol was present in the medium.

**Figure 6. Effect of proline concentration on $\Delta\Psi_{mt}$ and NADH autofluorescence of isolated mouse kidney mitochondria**. No substrates were present prior to addition of mitochondria. **(A-C)** Time course of safranine O signal indicative of $\Delta\Psi_{mt}$ (arbitrary units A.U.). Glutamate (G), malate (M), succinate (S), 1 μM SF and proline (Pro) added at the concentrations where indicated. **(A)** No targeted inhibition of electron transfer pathways. **(B)** Rotenone prior to addition of mitochondria. **(C)** Myxothiazol (Myx) prior to addition of mitochondria. **(D)** Time course of NADH autofluorescence (arbitrary units A.U.). Concentrations of Pro: black (a): 0 mM, red (b): 0.25 mM, green (c): 0.5 mM, orange (d): 2 mM, blue (e): 5 mM, magenta (f): 10 mM.

In accordance to the lower ProDH activities measured in brain and heart mitochondria (Figure 2A), addition of proline to brain (Figure 9A) or heart (Figure 9C) mitochondria led to a moderate gain of $\Delta\Psi_{mt}$. Accordingly, while measuring NADH autofluorescence or Q reduction, addition of proline to brain or heart mitochondria led to evanescent changes, see Figure panels 9B and 9D for NADH autofluorescence in brain and heart mitochondria and 9F for Q redox state in brain mitochondria, measured simultaneously with oxygen consumption rate (9E) and rhodamine 123 fluorescence (9G).
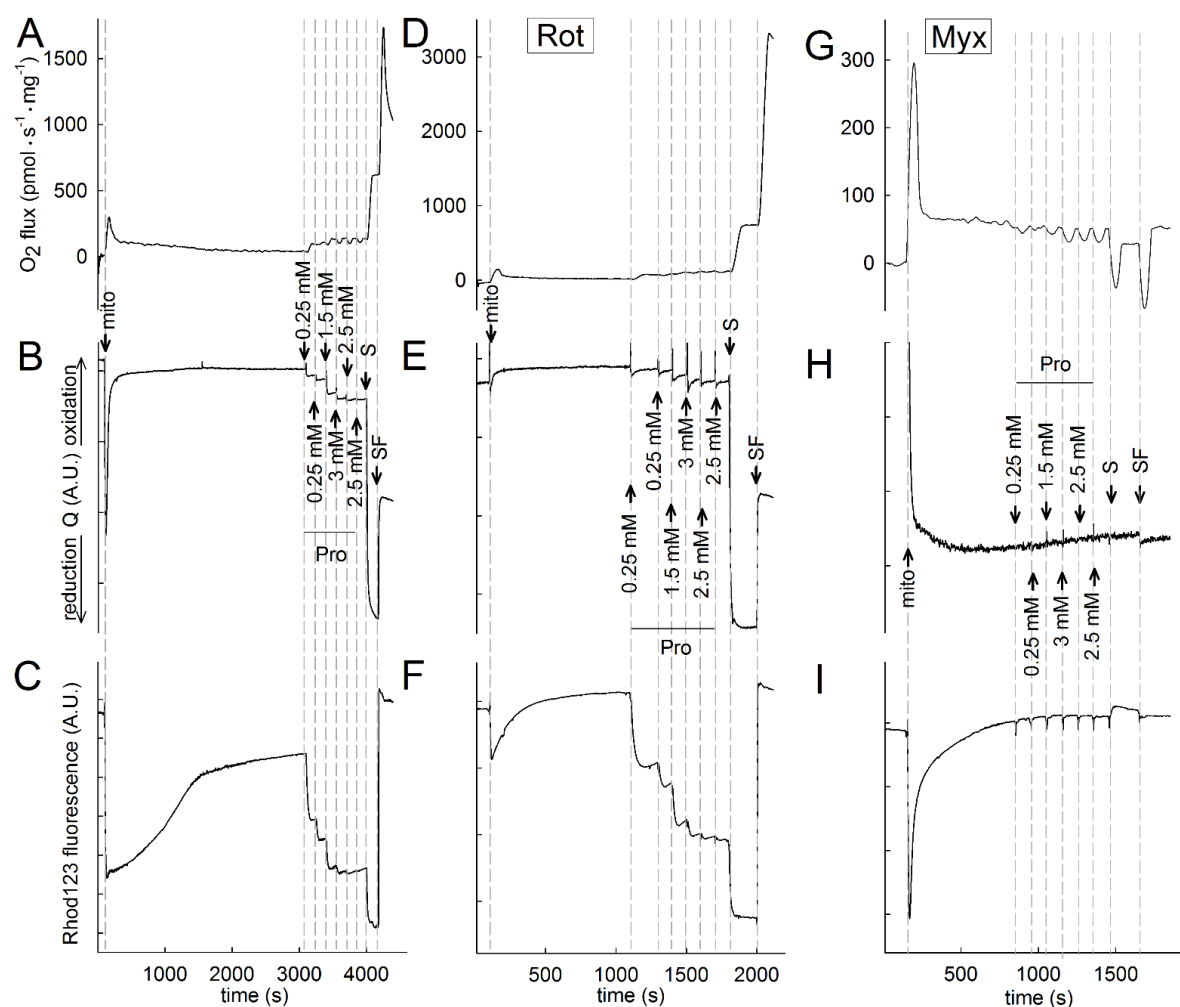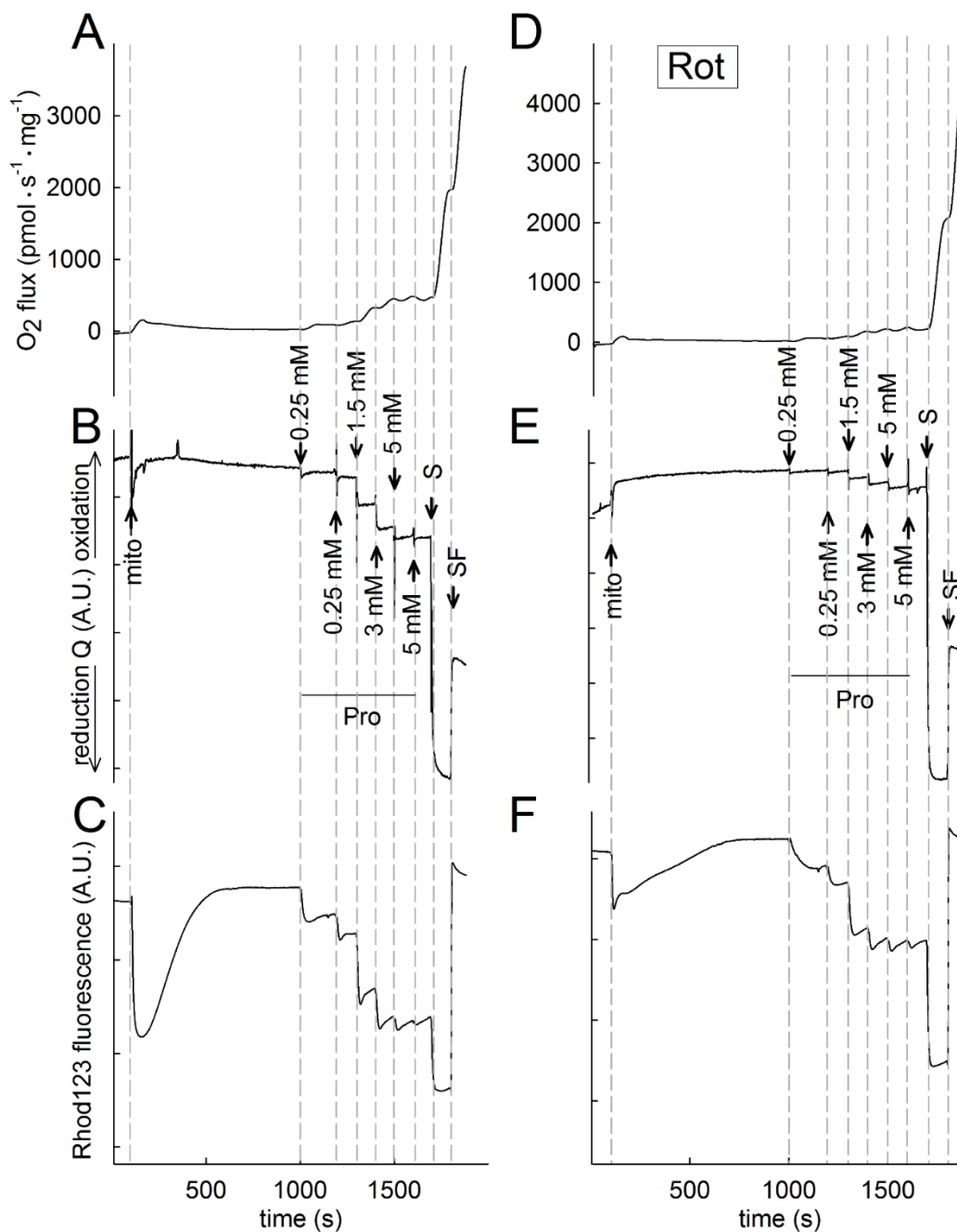
**Figure 7. Coenzyme Q (Q) redox state recorded simultaneously with oxygen consumption rate and rhodamine 123 fluorescence in isolated mouse kidney mitochondria using the NextGen-O2k**. No substrates were present before addition of mitochondria; proline (Pro) added at the concentrations indicated; succinate (S, 5 mM); 0.25 μM SF. **(A-C)** Time course of oxygen consumption, Q redox state, and rhodamine 123 fluorescence indicative of $\Delta\Psi_{mt}$ (arbitrary units A.U.), respectively. **(D-F)** As in A, B, and C, but with rotenone in the medium.
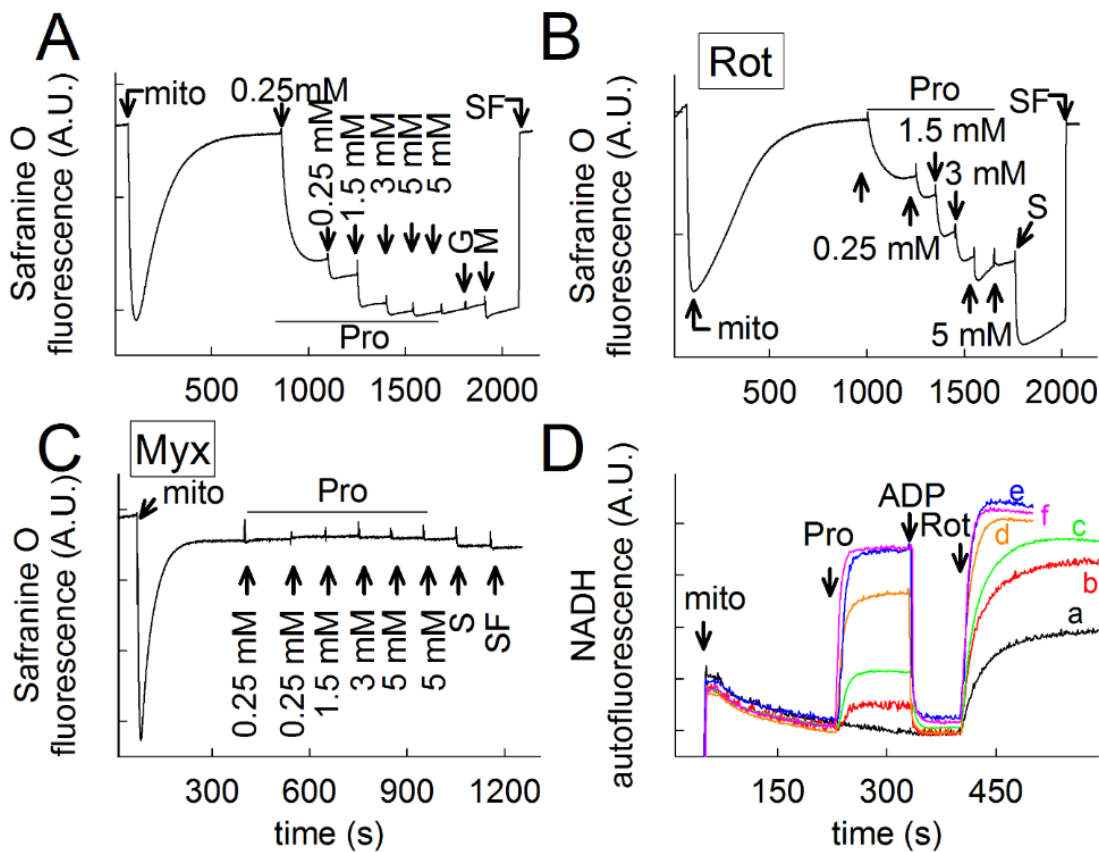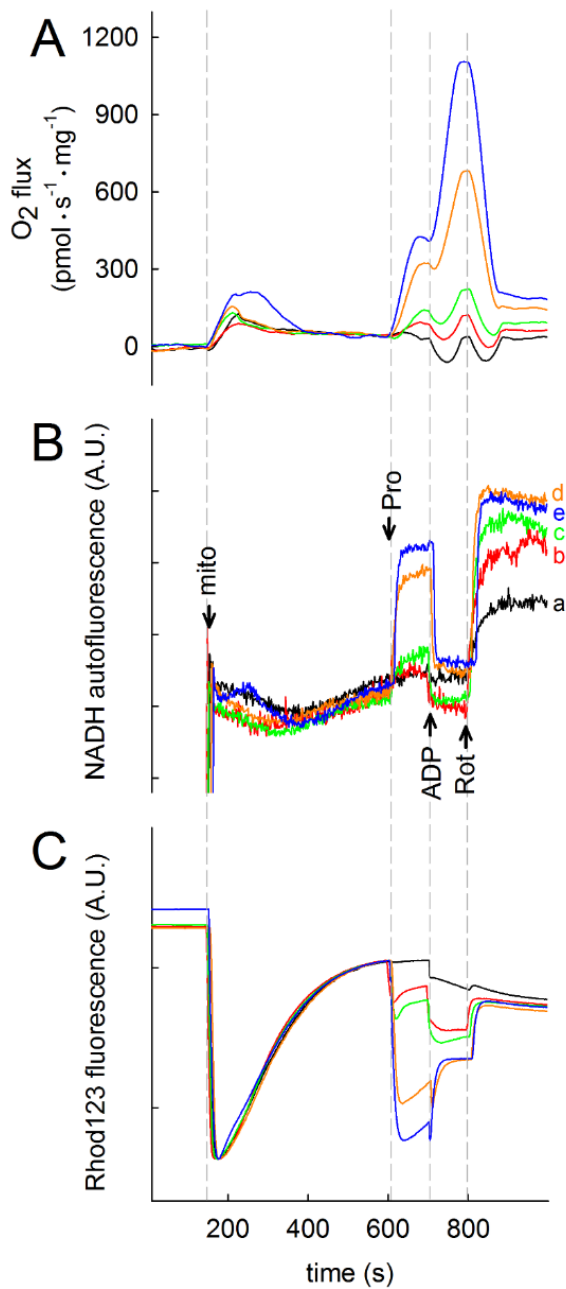
**Figure 8. Effect of proline concentration on respiration, $\Delta\Psi_{mt}$, and NADH autofluorescence of isolated mouse kidney mitochondria**. Time courses of **(A)** oxygen consumption, **(B)** NADH autofluorescence, and **(C)** rhodamine 123 fluorescence indicative of $\Delta\Psi_{mt}$ (arbitrary units A.U.), recorded simultaneously from the same kidney mitochondria using the NextGen-O2k and aligned on the dashed grey lines. No substrates were present prior to addition of mitochondria. Concentrations of proline (Pro): black (a): 0 mM, red (b): 0.25 mM, green (c): 0.5 mM, orange (d): 2 mM, blue (e): 5 mM.
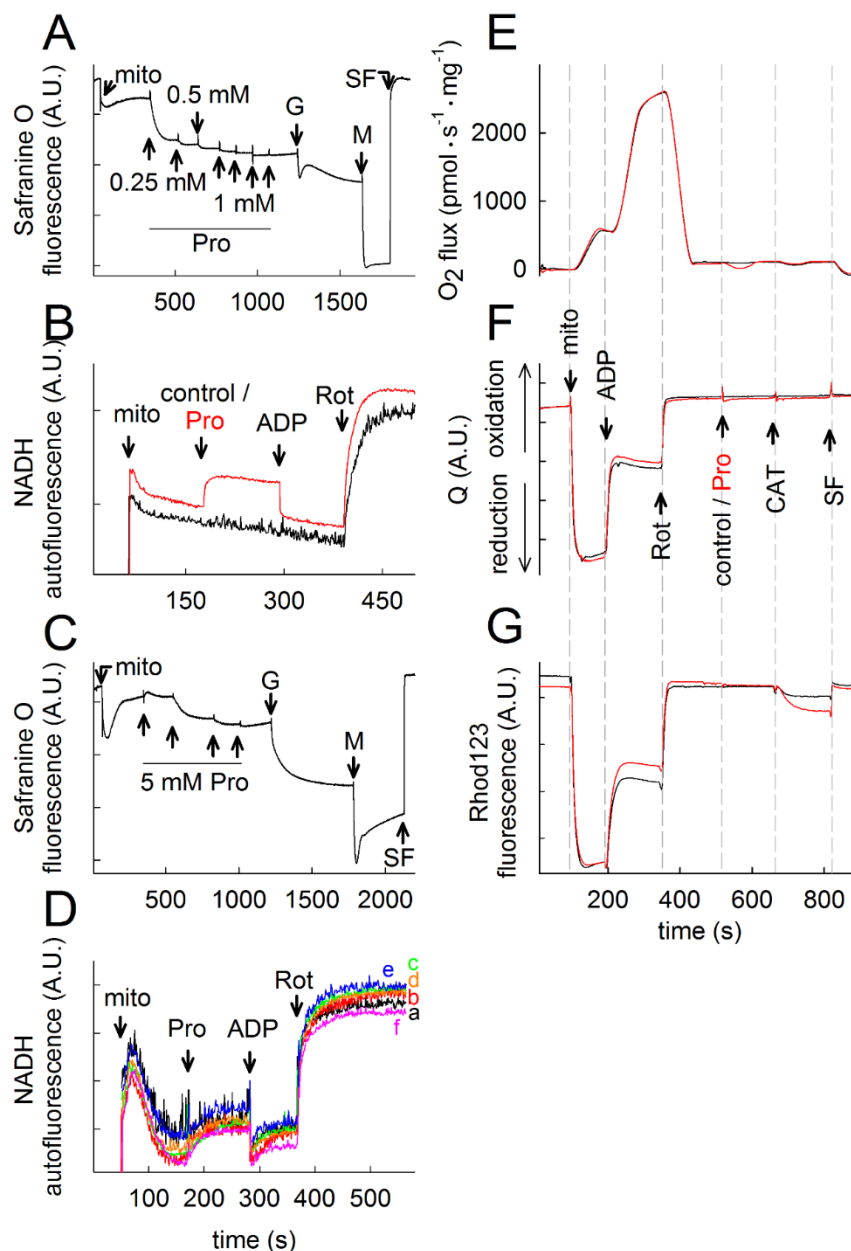
**Figure 9. Effect of proline concentration on ΔΨ$_{mt}$ and NADH autofluorescence of mitochondria isolated from (A, B) mouse brain and (C, D) mouse heart**. No substrates were present prior to addition of mitochondria; proline (Pro) added at the concentrations where indicated. **(A)** Time course of safranine O signal indicative of ΔΨ$_{mt}$ (arbitrary units A.U.). Glutamate (G) and malate (M) added where indicated. 1 μM SF. **(B)** Time course of NADH autofluorescence (arbitrary units A.U.). Red trace: 10 mM proline. **(C)** Time course of safranine O signal indicative of ΔΨ$_{mt}$ (arbitrary units A.U.). Glutamate (G) and malate (M) added where indicated. 1 μM SF. **(D)** Time course of NADH autofluorescence (arbitrary units A.U.). Pro: black (a): 0 mM, red (b): 1 mM, green (c): 2 mM, orange (d): 5 mM, blue (e): 10 mM, magenta (f): 20 mM. **(E-G)** Time courses of oxygen consumption, Q redox state and rhodamine 123 fluorescence indicative of ΔΨ$_{mt}$ (arbitrary

units A.U.), respectively, recorded simultaneously in the same brain mitochondria using the NextGen-O2k and aligned on the dashed grey lines. 0.25 µM SF. Black trace: GM; red trace: GM and 5 mM Pro.

## 2.5. Proline oxidation is sensitive to tetrahydro-2-furoic acid (THFA) and S-5-oxo-2-tetrahydrofurancarboxylic acid (S-5-oxo)

L-tetrahydro-2-furoic acid (THFA) and S-5-oxo-2-tetrahydrofurancarboxylic acid (S-5-oxo) have been described as specific inhibitors of ProDH [30], [31], the latter compound branded as "second-generation" from the former. In our hands, 10 mM THFA inhibited ProDH activity of liver and kidney mitochondria to a great extent (>80 % inhibition, see Figure panel 10A), while S-5-oxo had little -if any- effect at 5 mM. THFA exhibited a dose-dependent decrease in LEAK and OXPHOS respiration in both liver (10B) and kidney (10D) mitochondria. At 10 mM, S-5-oxo inhibited proline oxidation only in liver (Figure panel 10C) but not kidney (10E) mitochondria.
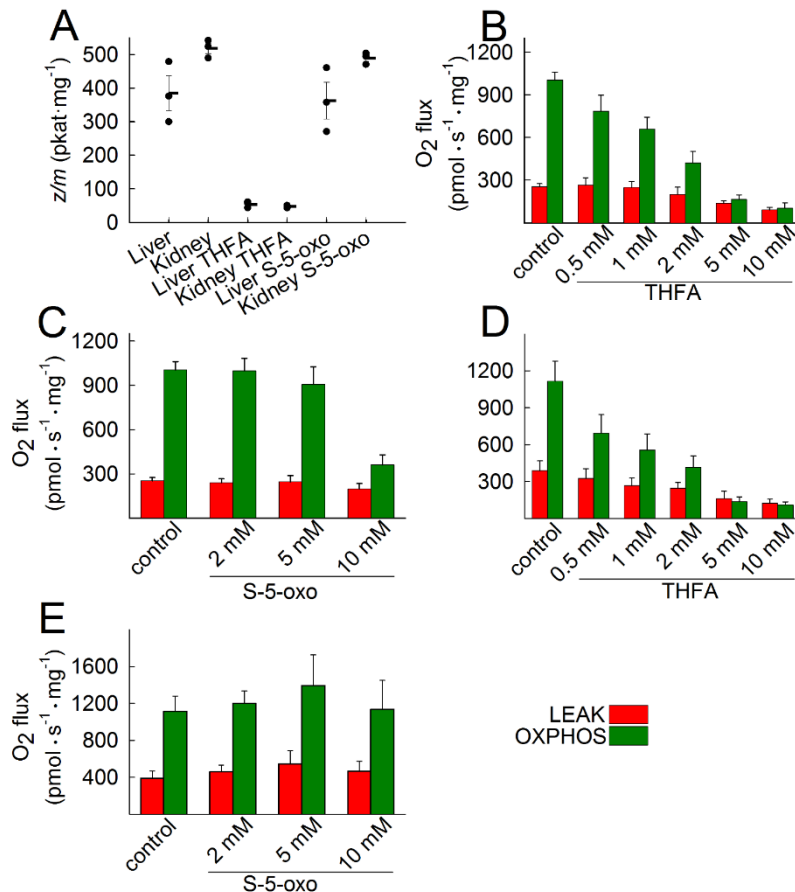


**Figure 10. The effects of THFA and S-5-oxo on ProDH activity and proline -mediated respiration rates in isolated mouse liver and kidney mitochondria**. **(A)** Scatter plot depicting ProDH catalytic activity (pkat/mg protein of isolated mitochondria) with 10 mM proline and the effects of THFA (10 mM) and S-5-oxo (5 mM). **(B)** Bar graph depicting LEAK (black) and OXPHOS (red) oxygen consumption rates in liver mitochondria respiring on 5 mM proline as a function of THFA concentration. **(C)** As in B but using S-5-oxo instead of THFA. **(D)** As in B, kidney mitochondria. **(E)** As in C, kidney mitochondria. Data are SEM of at least 3 independent experiments.

## 2.6. Effect of proline dehydrogenase inhibitors on proline-induced changes in Q redox state and ΔΨmt

Based on the inhibitory effects of THFA and S-5-oxo on ProDH activity and proline-mediated respiration, we sought to establish the effect of these inhibitors on other proline-mediated bioenergetic read-outs. For this, we investigated the effects of the compounds on proline-induced changes in Q redox state and $\Delta\Psi_{mt}$. As shown in Figure 11, in liver mitochondria THFA and S-5-oxo abolished the proline-induced Q reduction (proline added after ADP and the CI inhibitor rotenone) and decrease of rhodamine 123 fluorescence which is indicative of $\Delta\Psi_{mt}$. Q redox state and rhodamine fluorescence were recorded simultaneously to oxygen consumption and aligned on the dash grey lines. Results obtained from THFA are shown in 11A, B and C and from S-5-oxo in 11D, E and F. Various traces imply different substrate combinations and different concentrations of the ProDH inhibitor, detailed in the legend. Qualitatively similar results were obtained from kidney mitochondria, shown in Figure 12. In Figure panel 12A, the dose-dependent effect of THFA was examined in proline-induced changes of safranine O fluorescence indicative of $\Delta\Psi_{mt}$, while in Figure panels 12B, C and D recorded simultaneously using a NextGen-O2k (aligned in the grey dash lines) the effects of THFA in respiration, Q redox state and rhodamine 123 fluorescence are shown. Various traces imply different substrate combinations and different concentrations of the ProDH inhibitor, detailed in the legend.
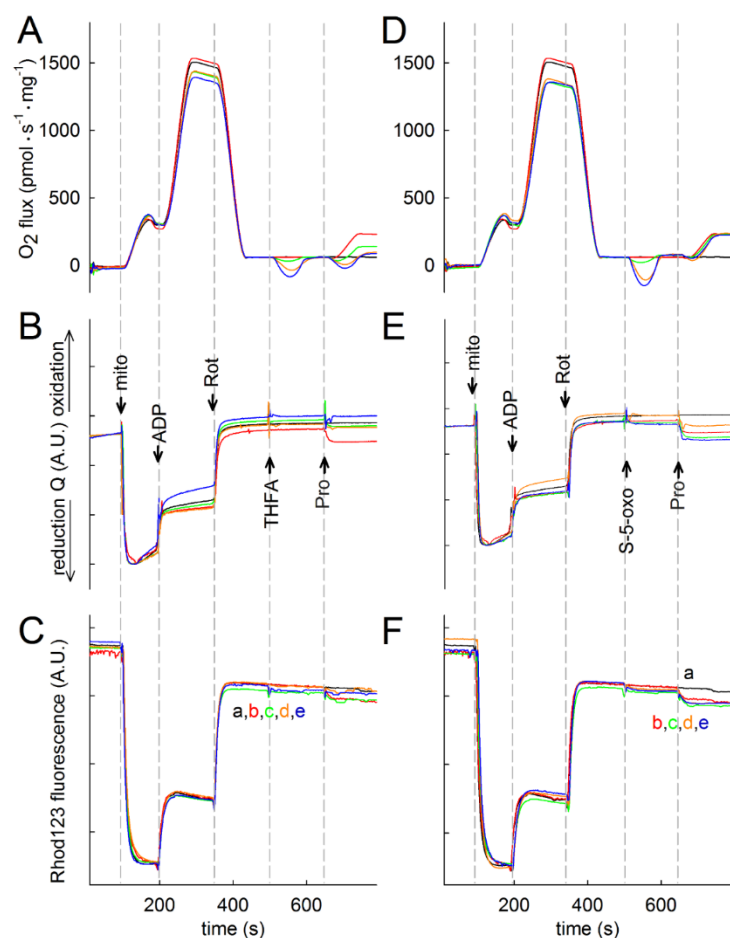


**Figure 11. The effects of THFA and S-5-oxo on oxygen consumption, Q redox state and rhodamine 123 fluorescence recorded simultaneously from the same liver mitochondria using the NextGen-O2k.** Proline (Pro, 5 mM), **(A-C)** THFA, **(D-F)** S-5-oxo. GMβOH always present: glutamate (G), malate (M), βOH (10 mM). Black (a): GMβOH; red (b): plus proline (Pro, 5 mM); green (c): plus Pro and THFA (2 mM) or S-5-oxo (2 mM); orange (d): plus Pro and THFA (5 mM) or S-5-oxo (5 mM); blue (e): plus Pro and THFA (10 mM) or S-5-oxo (10 mM).
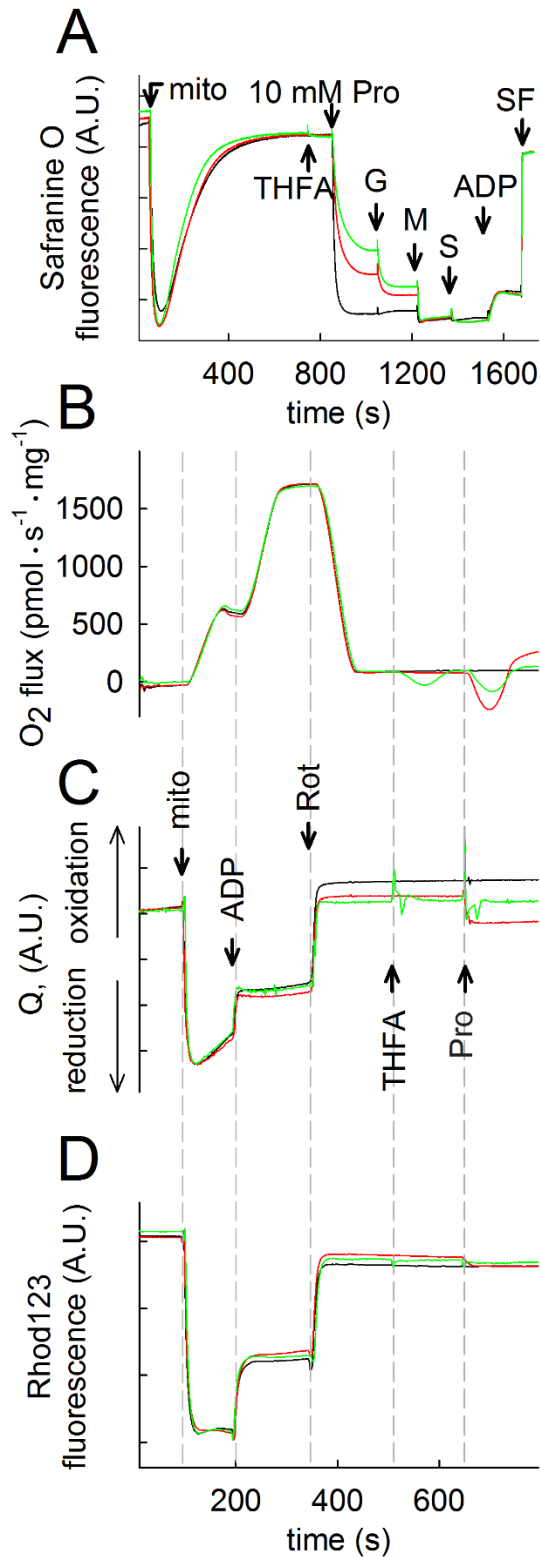
**Figure 12. The effects of THFA on kidney mitochondria**. **(A)** Time course of safranine O signal indicative of $\Delta\Psi_{mt}$ (arbitrary units, A.U.) in isolated kidney mitochondria. No substrates were present in the buffer prior to addition of mitochondria. Proline (Pro, 10 mM), glutamate (G), malate (M), succinate (S), ADP and 1 µM SF added where indicated. Red trace: plus 5 mM THFA; green trace: plus 10 mM THFA. (**B-D**) Time courses of oxygen consumption, Q redox state and rhodamine 123 fluorescence indicative of $\Delta\Psi_{mt}$ (arbitrary units A.U.), respectively, recorded simultaneously from the same kidney mitochondria using the NextGen-O2k and aligned on the dashed grey lines. GM and itaconate (10 mM) always present. Black traces: GM and itaconate (10 mM), red traces: plus 10 mM Pro; green traces: plus 10 mM proline and 10 mM THFA where indicated.

## 2.7. Effect of proline on ANT directionality

From the above experiments, it is evident that in mouse liver and kidney (and to a much lesser extent brain and heart) mitochondria and in accordance to corresponding ProDH activities, proline is catabolized generating $\Delta\Psi_{mt}$ in a manner dependent on CIII (and CIV) function. In order to address if this is sufficient for maintaining matrix ATP levels, we interrogated the directionality of ANT, a parameter which is profoundly sensitive to matrix [ATP]/[ADP] [32], [33], [18]. ANT directionality was addressed using a biosensor test developed by us, in which the effect of the ANT inhibitor carboxyatractyloside (CAT) is examined on $\Delta\Psi_{mt}$ during ADP-induced respiration but after targeted inhibition of the ETS [32]. Briefly, the adenine nucleotide exchange through the ANT is electrogenic, since 1 molecule of $ATP^{4-}$ is exchanged for 1 molecule of $ADP^{3-}$ [34]. In fully energized mitochondria, export of ATP in exchange for ADP costs ~25 % of the total energy produced [35]. Therefore, during the forward mode of ANT, abolition of its operation by CAT leads to a gain of $\Delta\Psi_{mt}$, whereas during the reverse mode of ANT, abolition of its operation by the inhibitor leads to $\Delta\Psi_{mt}$ loss.
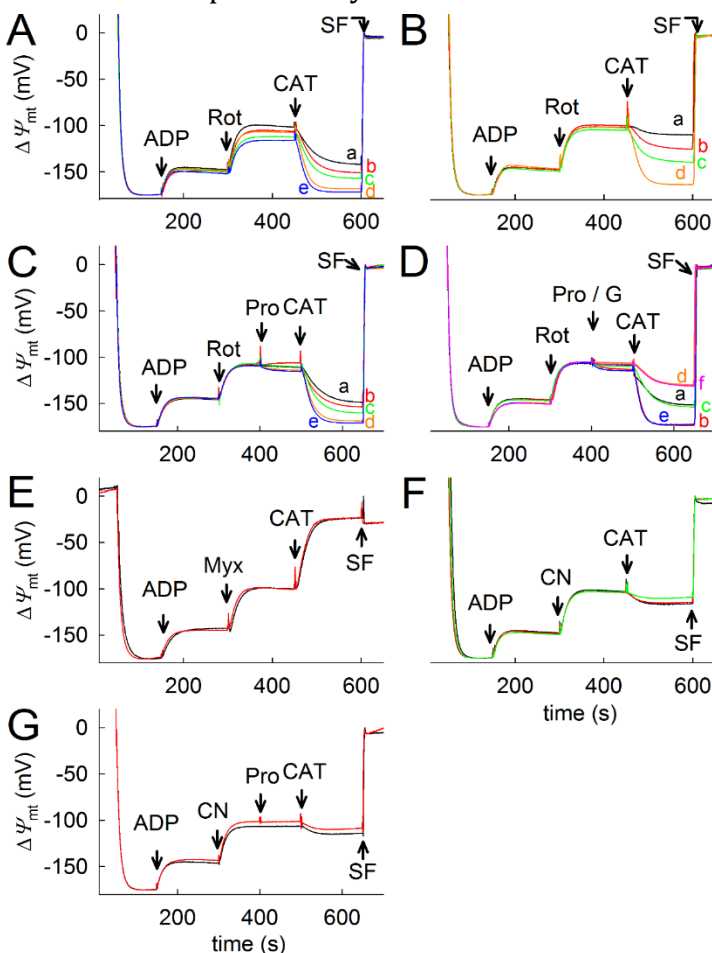


**Figure 13. The effect of proline on ANT directionality in isolated mouse liver mitochondria as a function of targeted inhibition of electron transfer pathways using various substrate-inhibitor combinations.** Traces are time courses of the safranine O signal calibrated to $\Delta\Psi_{mt}$. **(A)** GM always present plus increasing concentrations of proline (Pro); black (a): 0 mM; red (b): 0.25 mM; green (c): 0.5 mM; orange (d): 2 mM; blue (e): 5 mM. **(B)** As in A, but GM & 5 mM βOH always present. **(C)** As in A, but proline added after rotenone. **(D)** Black (a): GM; red (b): GM plus 5 mM Pro; green (c): GM plus additional 5 mM glutamate added where indicated; orange (d): GMβOH; blue (e): GMβOH plus 5 mM Pro added where indicated; magenta (f): GM and 5 mM βOH plus additional 5 mM glutamate added where indicated. **(E)** Black: GM; red: GM and 5 mM Pro added after myxothiazol (Myx). **(F)** black: GM; red: GM and 2 mM Pro; green: GM and 5 mM Pro; NaCN (CN, 1 mM) added where indicated. **(G)** black: GM; red: GM and 5 mM proline added after NaCN (CN, 1 mM).

A generalized scheme of this test is depicted in [36]. As shown in Figure panels 13, in mouse liver mitochondria proline kept the ANT operating in forward mode irrespective of the substrate combinations used and if it was present before or after ETS inhibition by rotenone (Figure panels 13A, B, C and D).
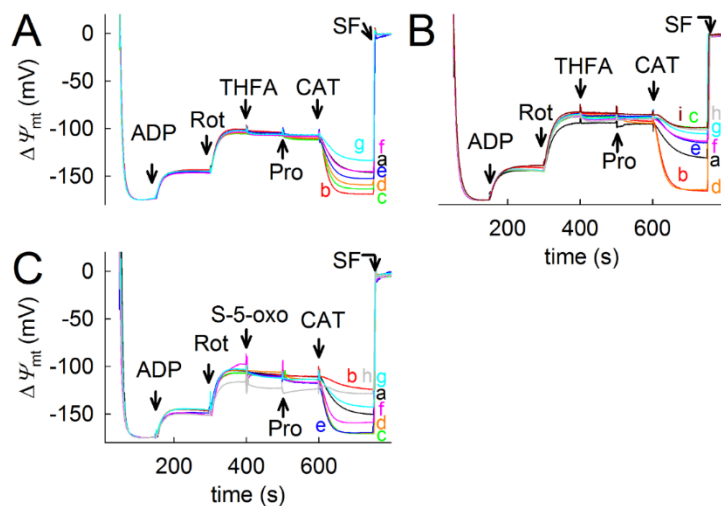


**Figure 14. The effect of THFA and S-5-oxo on proline-induced changes of ANT directionality in isolated mouse liver mitochondria**. Traces are time courses of safranine O signal calibrated to $\Delta\Psi_{mt}$. GM always contained in the medium. GMPro contains 5 mM proline. GMβOH contains 5 mM βOH, GMProβOH containes 5 mM Pro and 5 mM βOH. **(A)** Black (a): GM; red (b): GMPro; green (c): GMPro and 1 mM THFA; orange (d): GMPro and 2 mM THFA; blue (e): GMPro and 5 mM THFA; magenta (f): GMPro and 10 mM THFA; cyan (g): GM and 10 mM THFA. **(B)** Black (a): GM; red (b): GMPro; green (c): GMβOH; orange (d): GMProβOH; blue (e): GMProβOH and 10 mM THFA; magenta (f): GMProβOH and 15 mM THFA; cyan (g): GMProβOH and 20 mM THFA; grey (h): GMProβOH and 25 mM THFA; brown (i): GM and 25 mM THFA. **(C)** Black (a): GM; red (b): GMβOH; green (c): GMPro; orange (d): GMProβOH; blue (e): GMProβOH and 10 mM S-5-oxo; magenta (f): GMProβOH and 15 mM S-5-oxo; cyan (g): GM and 10 mM S-5-oxo; grey (h): GM and 15 mM S-5-oxo.

However, when ETS was blocked at the level of CIII with myxothiazol (Myx, panel 13E) or CIV with cyanide (CN, panels 13F, G), proline failed to maintain the ANT in forward mode, implying that any changes conferred by proline required the uninterrupted operation of both CIII and CIV. Importantly, an excess of glutamate could not reproduce the effects of proline (panel 13D), indicating that the effects of proline are not due to downstream formation of glutamate. As expected, the effects of proline in liver mitochondrial ANT directionality were sensitive to inhibition by both THFA (Figure panel 14A, B) and S-5-oxo (panel 14C). Qualitatively similar results were obtained with kidney (Figures 15 and 16), brain (Figure 17) and heart (Figure 18) mitochondria, always in accordance to ProDH activities; however, S-5-oxo was much less potent than THFA in kidney mitochondria. In experiments using kidney mitochondria, 2-ketobutyrate was also included; 2-ketobutyrate negates mSLP due to the ATP-consuming propionyl-CoA carboxylase step [37], and this was used so as to limit mSLP and examine any beneficial effects of proline that could be affected by the ProDH inhibitors. As also expected, proline had no effect on ANT directionality of mitochondria subject to anoxia (i.e. complete non-pharmacological CIV inhibition), see figure 19. Interestingly, proline exhibited a dose-dependent effect in CAT-induced Q reduction in the presence of glutamate and malate (Figure 20B) which was dampened if βOH was concomitantly present (20E). These

recordings were simultaneously made with oxygen consumption rate and rhodamine 123 fluorescence (indicative of $\Delta\Psi_{mt}$) (Figure panels 20A, D and 20C, F, respectively) using the NextGen-O2k, in isolated liver mitochondria. Qualitatively similar results were obtained with kidney mitochondria (Figure 22). The reason(s) of this CAT-induced changes in Q redox state during CI inhibition and as a function of proline were not investigated further. As expected, when CIII was inhibited by myxothiazol (Figure 21) or under anoxia (Figure 21) these phenomena were not observed. Qualitatively similar results were obtained with anoxic (figure 23) and CIII-inhibited kidney mitochondria (Figure 22E).
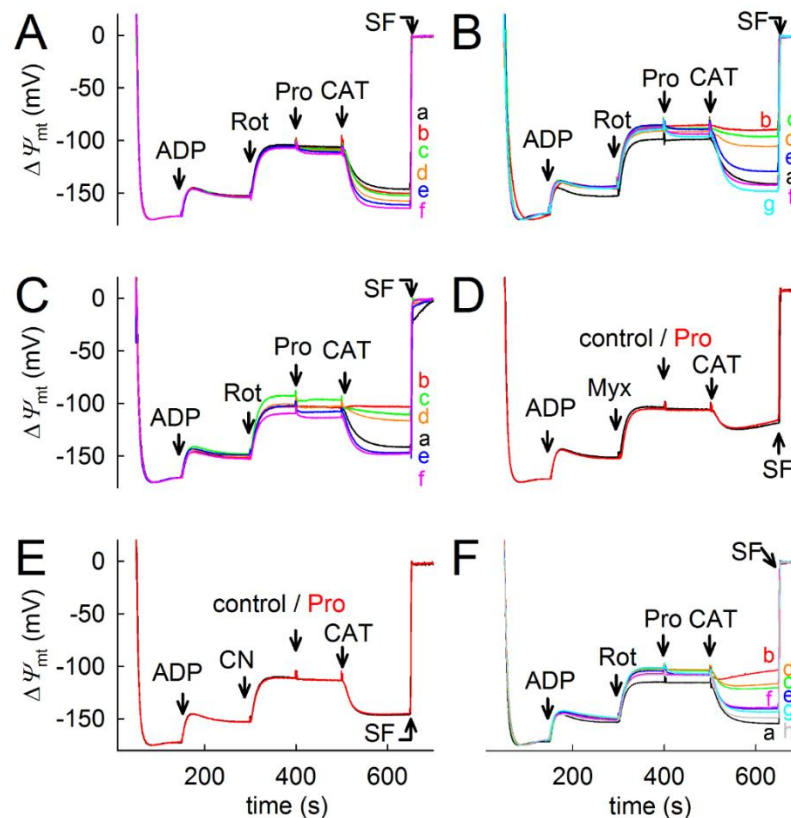


**Figure 15. The effect of proline on ANT directionality in isolated mouse kidney mitochondria as a function of targeted inhibition of electron transfer pathways using various substrate-inhibitor combinations**. Traces are time courses of safranine O signal calibrated to $\Delta\Psi_{mt}$. GM always contained in the medium. Itaconate (Itac, 5 mM), ketobutyrate (2 mM) where indicated. **(A)** Black (a): GM; red (b): GM and 0.25 mM proline (Pro); green (c): GM and 0.5 mM Pro; orange (d): GM and 2 mM Pro; blue (e): GM and 5 mM Pro; magenta (f): GM and 10 mM Pro. **(B)** Black (a): GM; red (b): GM & itaconate; green (c): GM & itaconate and 0.25 mM Pro; orange (d): GM & itaconate and 0.5 mM Pro; blue (e): GM & itaconate and 2 mM Pro; magenta (f): GM & itaconate and 5 mM Pro; cyan (g): GM & itaconate and 10 mM Pro. **(C)** Black (a): GM; red (b): GM & ketobutyrate; green (c): GM & ketobutyrate and 0.25 mM Pro; orange (d): GM & ketobutyrate and 0.5 mM Pro; blue (e): GM & ketobutyrate and 2 mM Pro; magenta (f): GM & ketobutyrate and 5 mM

proline. **(D)** Black trace: GM; red trace: GM and 10 mM proline added after myxothiazol (Myx). **(E)** Black trace: GM; red trace: GM and 10 mM proline added after NaCN (CN, 1 mM). **(F)** As in B, but in traces d, f and h proline was present in the media prior to addition of mitochondria. Black (a): GM present in the buffer; red (b): GM and Itac present in the buffer; green (c): GM and Itac present in the buffer, 0.5 mM Pro added at 400 s; orange (d): GM, Itac and 0.5 mM Pro present in the buffer from the begining; blue (e): GM and Itac present in the buffer; 2mM Pro added at 400 s; magenta (f): GM, Itac and 2 mM Pro present in the buffer from the beginning; cyan (g): GM and Itac present in the buffer, 5 mM Pro added at 400 s; silver (h): GM, Itac and 5 mM Pro present in the buffer from the beginning.
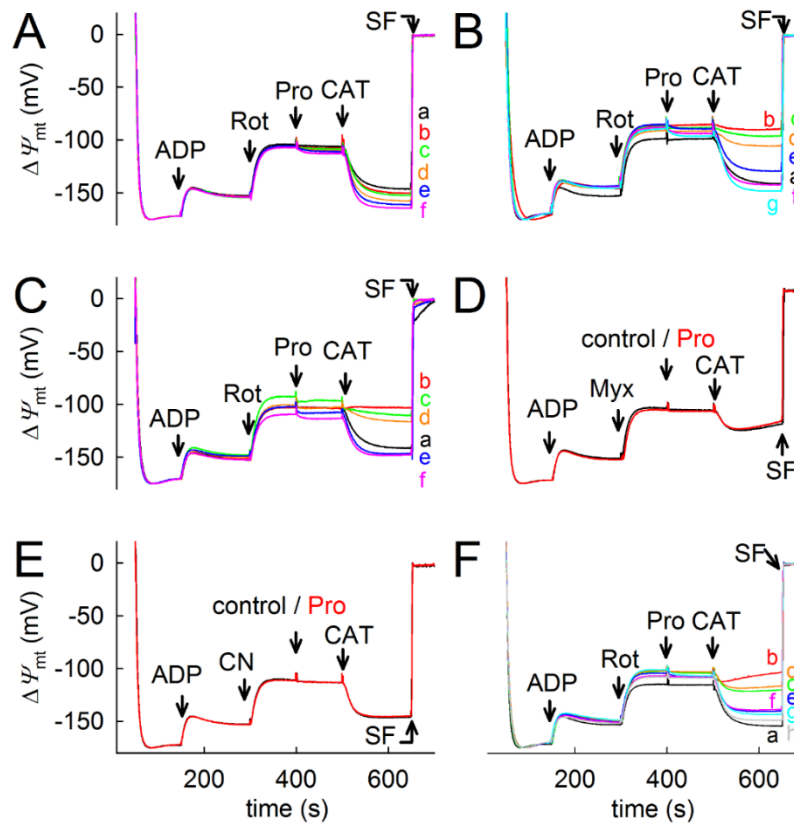


**Figure 16. The effect of THFA and S-5-oxo on proline-induced changes of ANT directionality in isolated mouse kidney mitochondria**. Traces are time courses of safranine O signal calibrated to $\Delta\Psi_{mt}$. GM always contained in the medium. Proline (Pro, 10 mM) where indicated. **(A)** Itaconate (2 mM) where indicated. Black (a): GM; red (b): GM & itaconate; green (c): GM & proline; orange (d): GM & proline & itaconate; blue (e): GM & proline & itaconate and 1 mM THFA; magenta (f): GM & proline & itaconate and 2 mM THFA; cyan (g): GM & proline & itaconate and 5 mM THFA; grey (h): GM & proline & itaconate and 10 mM THFA; brown (i): GM & proline & itaconate and 15 mM THFA. **(B)** Itaconate (6 mM) where indicated. Black (a): GM; red (b): GM & itaconate; green (c): GM & proline; orange (d): GM & proline & itaconate; blue (e): GM & proline & itaconate and 10 mM S-5-oxo; magenta (f): GM and 10 mM S-5-oxo.

**Figure 17. The effect of proline on ANT directionality in isolated mouse brain mitochondria**. Traces are time courses of safranine O signal calibrated to $\Delta\Psi_{mt}$. Pyruvate (P, 5 mM), glutamate (G), malate (M), βOH (2 mM), itaconate (2 mM) where indicated. **(A)** Black (a): GM; red (b): GM and 0.25 mM proline (Pro); green (c): GM and 0.5 mM Pro; orange (d): GM and 2 mM Pro; blue (e): GM and 5 mM Pro; magenta (f): GM and 10 mM Pro. **(B)** Black (a): GM; red (b): GM & itaconate; green (c): GM & itaconate and 2 mM Pro; orange (d): GM & itaconate (2 mM) and 5 mM Pro; blue (e): GM & itaconate and 10 mM Pro. **(C)** Black trace: G; red trace: G & 5 mM Pro; green trace: G & 10 mM Pro. **(D)** Black trace: P; red trace: P & 5 mM Pro. **(E)** Black (a): GM; red (b): GMβOH; green (c): GMβOH & 0.25 mM Pro; orange (d): GMβOH & 0.5 mM Pro; blue (e): GMβOH & 2 mM Pro; magenta (f): GMβOH & 5 mM Pro.

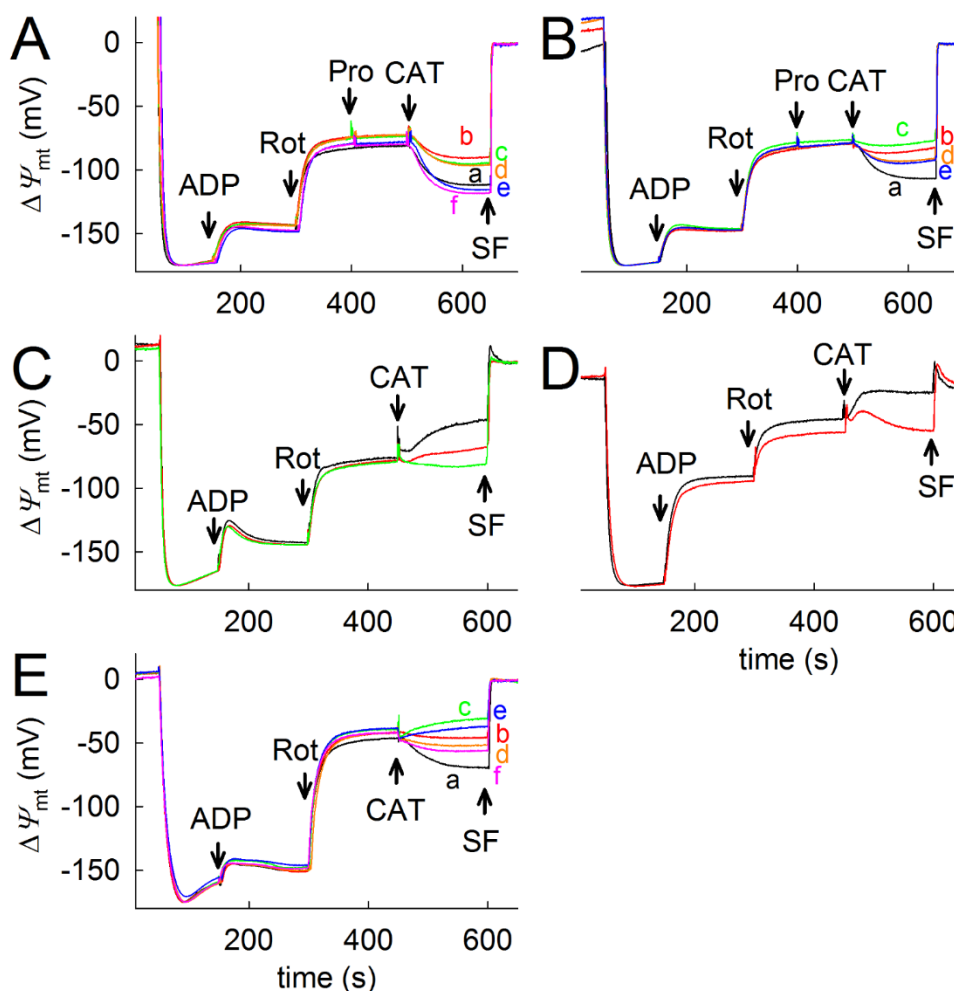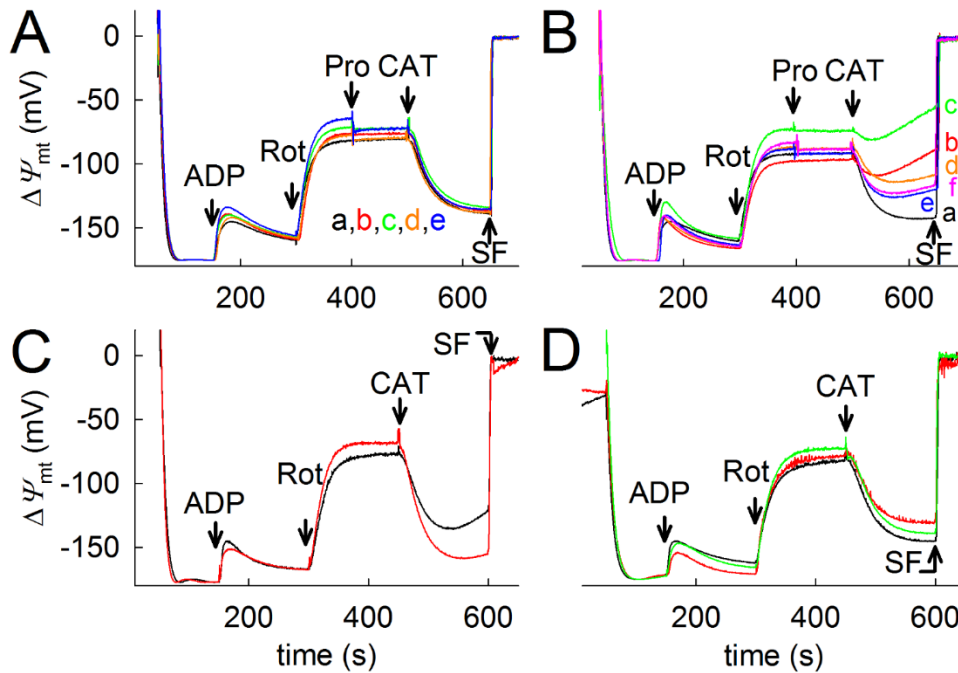**Figure 18. The effect of proline on ANT directionality in isolated mouse heart mitochondria**. Traces are time courses of safranine O signal calibrated to $\Delta\Psi_{mt}$. βOH (5 mM), where indicated. **(A)** GM always contained in the medium, increasing concentrations of proline (Pro); black (a): 0 mM; red (b): 5 mM; green (c): 10 mM; orange (d): 20 mM; blue (e): 40 mM. **(B)** GM always present in the medium, 5 mM itaconate (Itac) present in the medium when indicated, Pro added where indicated. Black trace (a): GM; red (b): GM and Itac; green (c): GM, Itac and 5 mM Pro; orange (d): GM, Itac and 10 mM Pro; blue (e): GM, Itac and 20 mM Pro; magenta (f): GM, Itac and 30 mM Pro. **(C)** Black trace: G; red trace: G & 5 mM Pro. **(D)** Black trace: GM; red trace: GMβOH; green trace: GMβOH & 5 mM Pro.

## 2.8. Proline oxidation maintains $F_1F_0$-ATPase in forward mode during Complex I inhibition

When mitochondria respire on pyruvate or other widely used NADH-linked substrates such glutamate or oxoglutarate, inhibition of the electron transport system at the level of CI leads to $F_1F_0$-ATPase reversal [38], [39]. This results in the maintenance of a $\Delta\Psi_{mt}$ value not higher than the reversal potential of the $F_1F_0$-ATPase [33], [18]. Mindful that proline fuels mitochondria through ProDH reducing Q reminiscent of CI bypass [40], [41], we sought to address the directionality of $F_1F_0$-ATPase in mitochondria supported by proline in the presence of the CI inhibitor rotenone. This was done in a manner similar to interrogating ANT directionality but using the $F_1F_0$-ATPase inhibitor oligomycin (Omy) instead of CAT. As shown in Figure 24 for liver and Figure 25 for kidney mitochondria, proline -added in various concentrations as indicated in the legends- maintained $F_1F_0$-ATPase in forward mode; this was not observed if CIII was inhibited by myxothiazol (Myx, panel 24E, 25F) or CIV was inhibited by cyanide (CN, panel 24F, 25G).
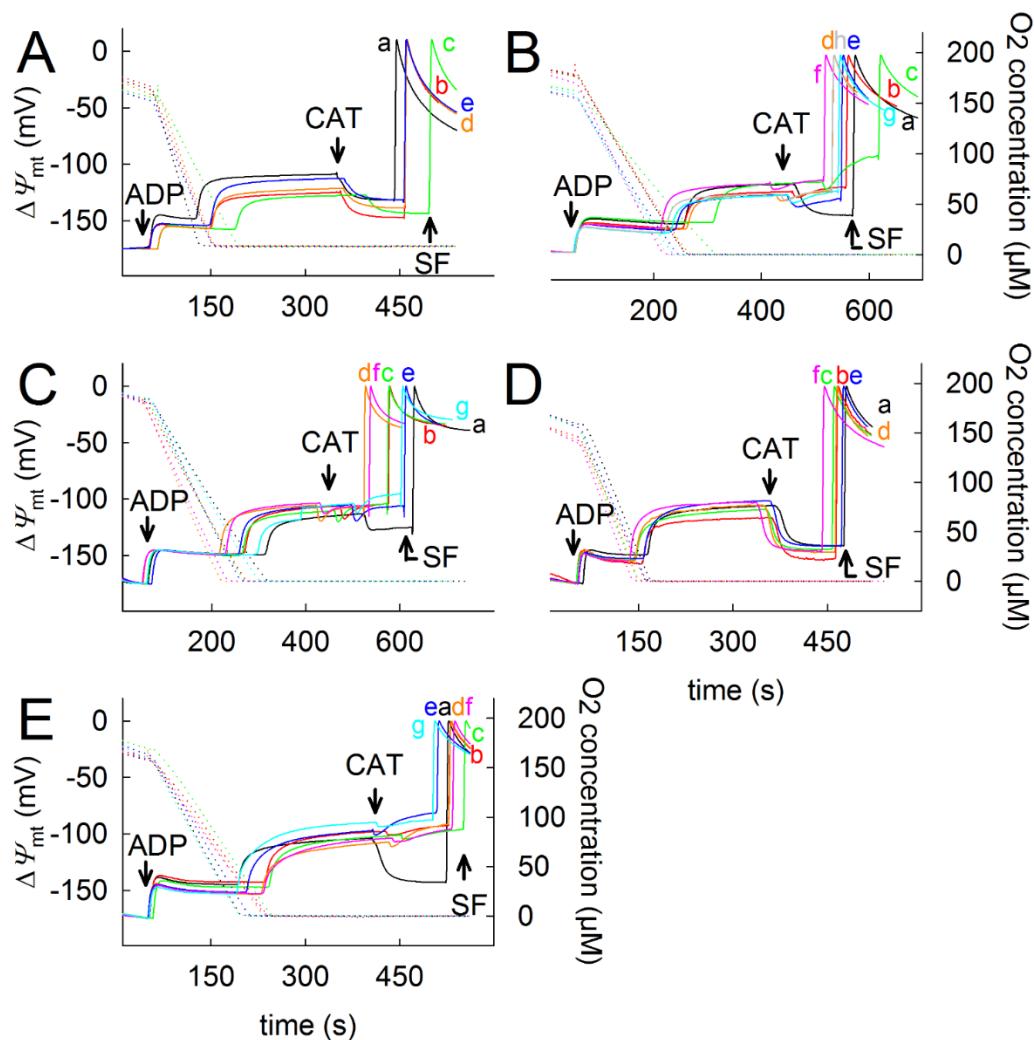
**Figure 19. Lack of effect of proline on ANT in anoxic mouse liver (A-C) and kidney (D, E) mitochondria**. Traces are time courses of simultaneous measurements of safranine O signal calibrated to $\Delta\Psi_{mt}$ (solid lines) and oxygen concentration in the media (dotted lines). GM always contained in the medium. **(A)** GM and increasing concentrations of Pro; black (a): 0 mM; red (b): 0.25 mM; green (c): 0.5 mM; orange (d): 2 mM; blue (e): 5 mM. **(B)** GM or GM & itaconate (1 mM or 2 mM in traces b to h), and increasing concentrations of Pro; black (a): 0 mM; red (b): 1 mM itaconate & 0 mM; green (c): 2 mM itaconate & 0 mM; orange (d): 1 mM itaconate & 0.25 mM; blue (e): 1 mM itaconate & 0.5 mM; magenta (f): 1 mM itaconate & 2 mM; cyan (g): 1 mM itaconate & 5 mM; grey (h): 1 mM itaconate & 10 mM. **(C)** GM or GM & βOH in traces b to g, and increasing concentrations of Pro; black (a): 0 mM; red (b): 0 mM; green (c): 0.25 mM; orange (d): 0.5 mM; blue (e): 2 mM; magenta (f): 5 mM; cyan (g): 10 mM. **(D)** GM and increasing concentrations of Pro; black (a): 0 mM; red (b): 0.25 mM; green (c): 0.5 mM; orange (d): 2 mM; blue (e): 5 mM; magenta (f): 10 mM. **(E)** GM (a) or GM & itaconate in traces b to g, and increasing concentrations of Pro; black (a): 0 mM; red (b): 0 mM; green (c): 0.25 mM; orange (d): 0.5 mM; blue (e): 2 mM; magenta (f): 5 mM; cyan (g): 10 mM.

**Figure 20. The effect of proline on CAT-induced changes in respiration (A, D) and Q redox state (B, E), and rhodamine 123 fluorescence (C, F) indicative of $\Delta\Psi_{mt}$ (arbitrary units A.U.) measured simultaneously in the same mouse liver mitochondria using the NextGen-O2k and aligned on the dashed grey lines**. GM always contained in the medium; 0.25 μM SF. **(A-C)** GM and increasing concentrations of Pro; black (a): 0 mM; red (b): 0.25 mM; green (c): 0.5 mM; orange (d): 2 mM; blue (e): 5 mM; magenta (f): 10 mM. **(D-F)** 5 mM βOH is additionally present in traces b-f, and increasing concentrations of Pro; black (a): 0 mM; red (b): 0 mM; green (c): 0.25 mM; orange (d): 0.5 mM; blue (e): 2 mM; magenta (f): 5 mM.

**Figure 21. No effect of proline on Q redox state of mitochondria inhibited at CIII (myxothiazol, 0.1 μM) or under anoxia (E)**. Oxygen consumption **(A)** or concentration **(D)**, Q redox state **(B, E)**, and rhodamine 123 fluorescence **(C, F)** indicative of $\Delta\Psi_{mt}$ (arbitrary units A.U.) measured simultaneously in the same mouse liver mitochondria using the NextGen-O2k and aligned on the dashed grey lines. Black traces: GM (& 10 mM βOH in B, D, F); red trace: GM plus 5 mM proline where indicated (& 10 mM βOH in B, D, F). 0.25 μM SF.
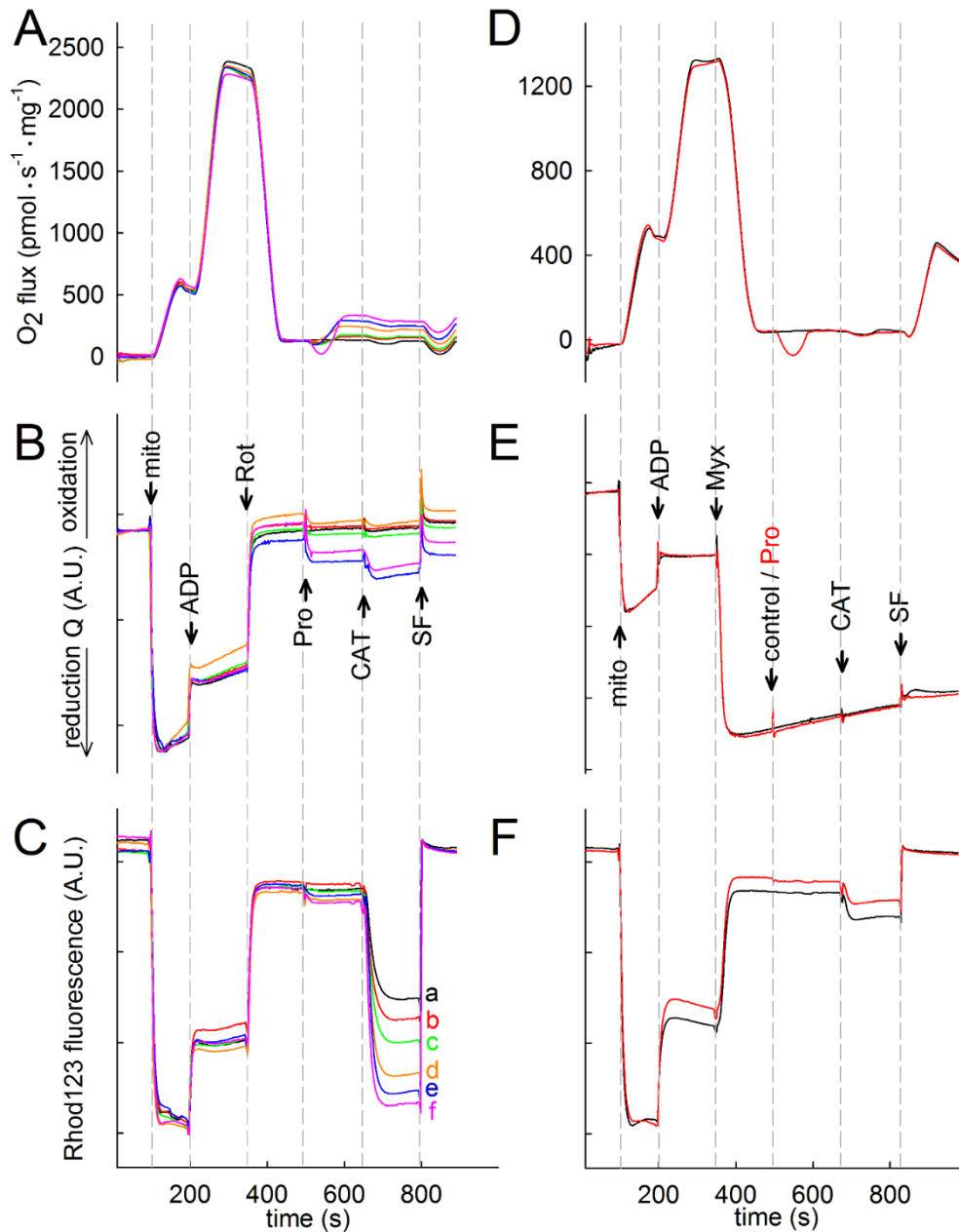
**Figure 22. The effect of proline on CAT-induced changes in Q redox state and its abolition by myxothiazol**. Oxygen consumption rate **(A, D)**, Q redox state **(B, E)**, and rhodamine 123 fluorescence **(C, F)** indicative of $\Delta\Psi_{mt}$ (arbitrary units A.U.) measured simultaneously in the same mouse kidney mitochondria using the NextGen-O2k and aligned on the dashed grey lines. 0.25 μM SF. **(A-C)** Rotenone (Rot), GM and increasing concentrations of Pro; black (a): 0 mM; red (b): 0.25 mM; green (c): 0.5 mM; orange (d): 2 mM; blue (e): 5 mM; magenta (f): 10 mM. **(D-F)** Myxothiazol (Myx, 0.1 μM). Black traces: GM & 10 mM itaconate; red traces: 10 mM Pro added where indicated.
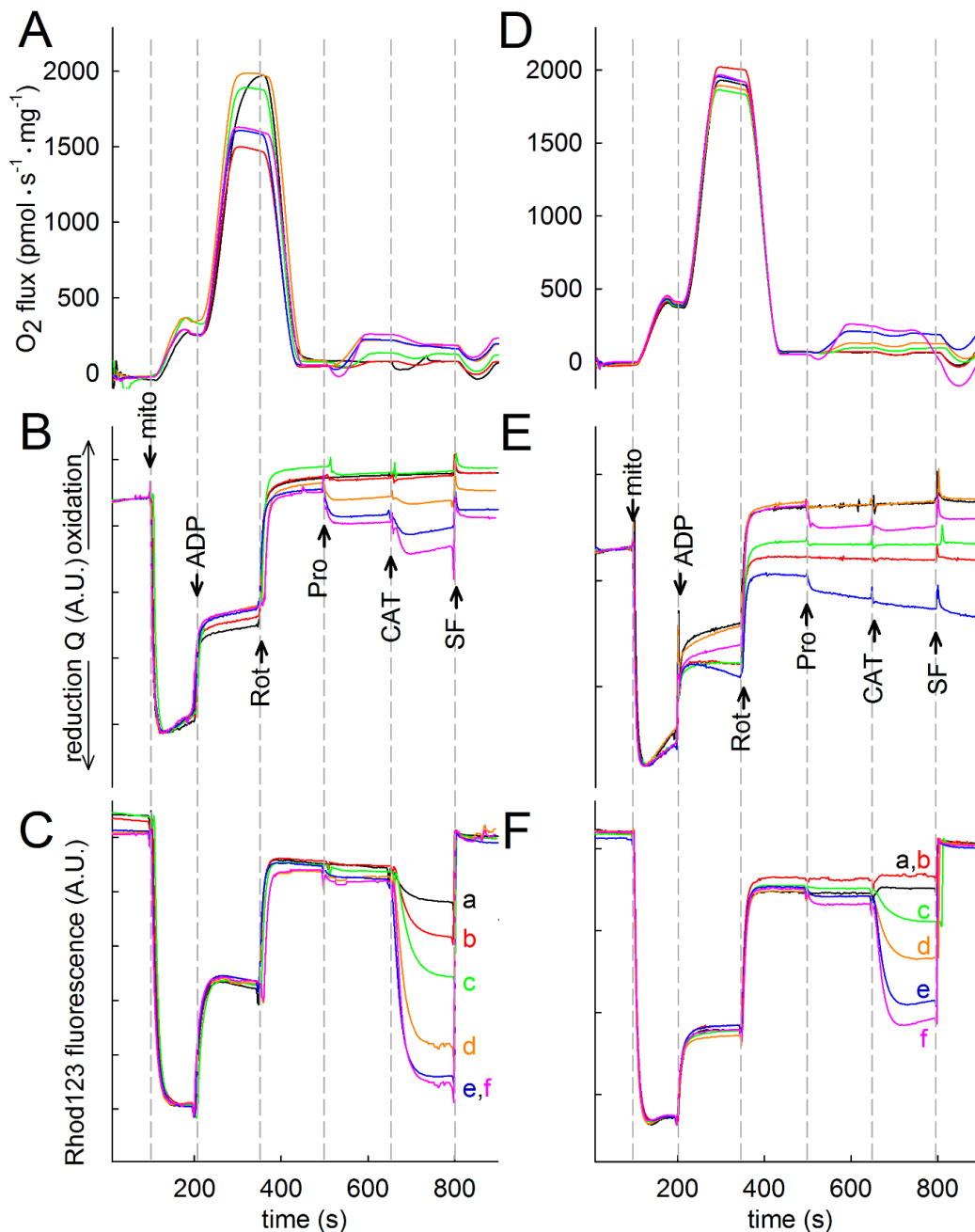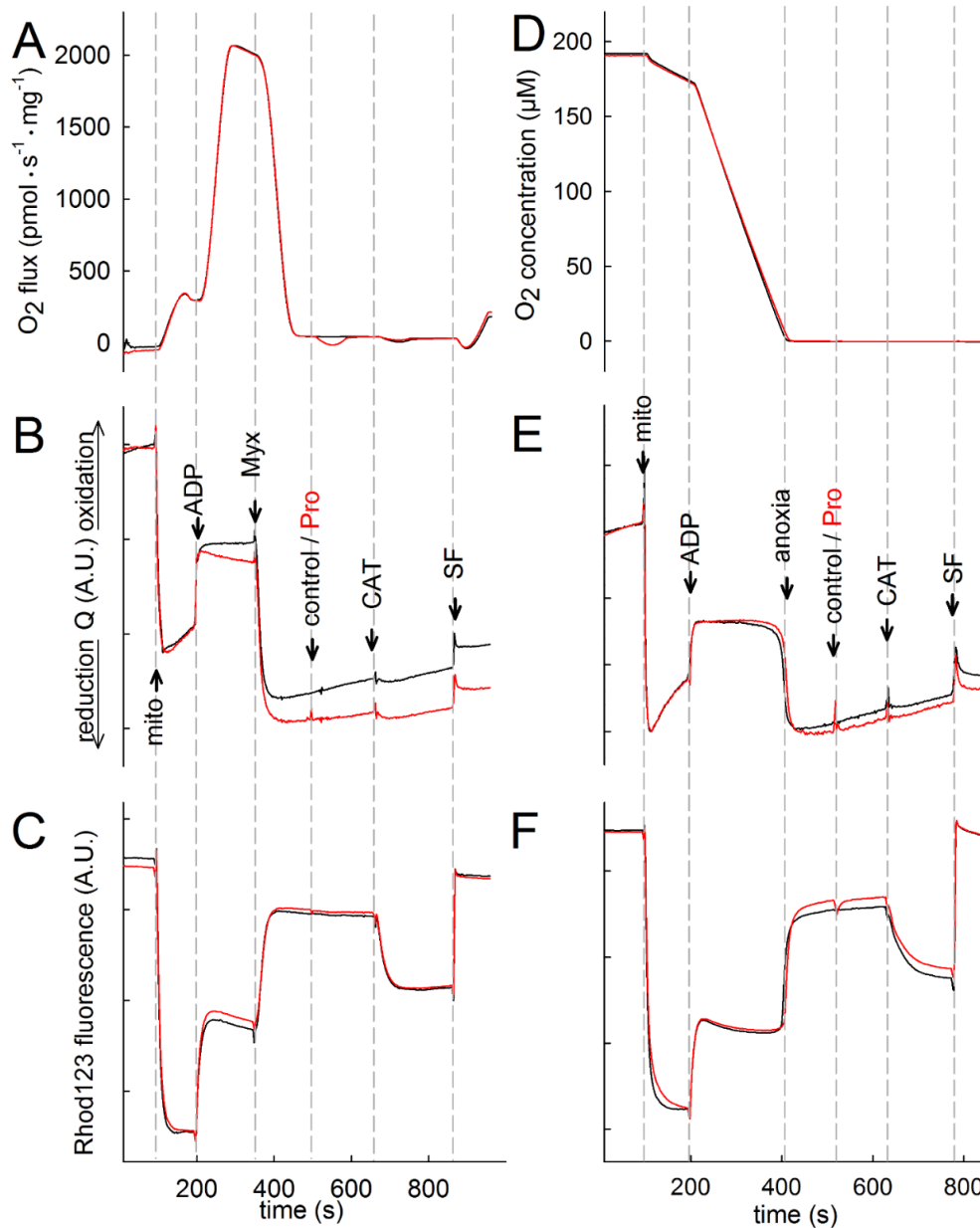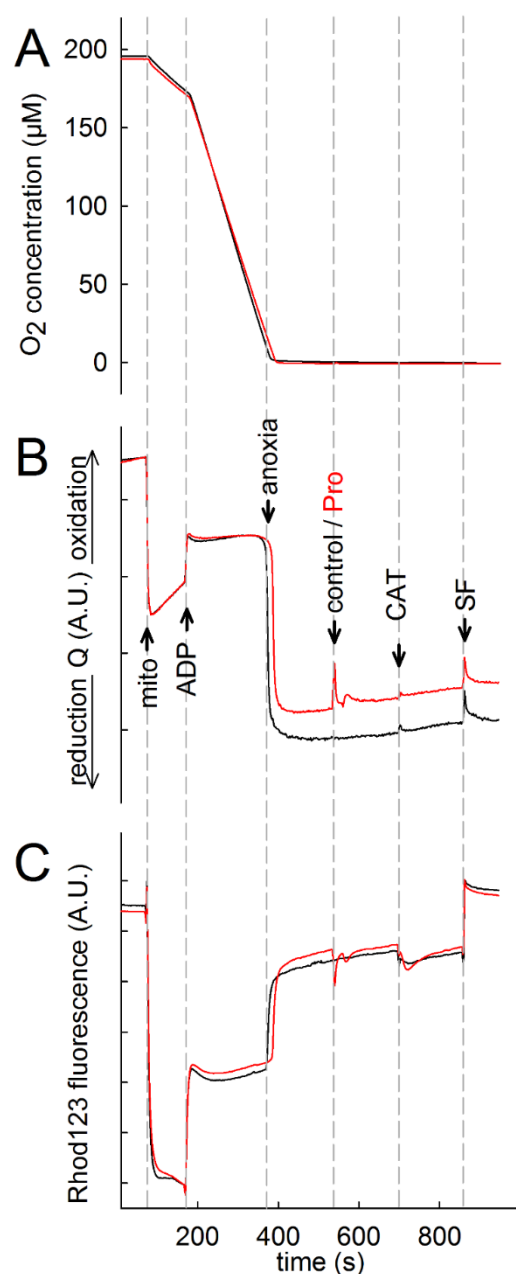
**Figure 23. No effect of proline on Q redox state of anoxic kidney mitochondria**. Oxygen concentration **(A)**, Q redox state **(B)**, and rhodamine 123 fluorescence **(C)** indicative of $\Delta\Psi_{mt}$ (arbitrary units A.U.) measured simultaneously in the same mouse kidney mitochondria using the NextGen-O2k and aligned on the dashed grey lines. Black traces: GM & 5 mM itaconate; red traces: GM & 5 mM itaconate plus 10 mM proline added where indicated. 0.25 µM SF.

In agreement with the data above, this effect of proline was abolished by THFA (panel 24G, 25C, 25D). Importantly, the effect of proline maintaining $F_1F_0$-ATPase operation in forward mode was primarily due to a small but sufficient gain in $\Delta\Psi_{mt}$, effectively crossing the reversal potential of the $F_1F_0$-ATPase "to the left", see [36]. This was deduced from the experiments shown in Figure panel 24D for liver and 25E for kidney mitochondria. In these experiments, the uncoupler SF6847 was titrated to clamp $\Delta\Psi_{mt}$ to a level equal just before proline addition. Indeed, at these SF6847 concentrations, the effect of proline was abolished. From this, we concluded that proline was maintaining $F_1F_0$-ATPase in forward mode exclusively because of a gain in $\Delta\Psi_{mt}$ due to proton pumping by CIII and CIV, supported by Q reduction through ProDH.

**Figure 24. The effect of proline on $F_1F_0$-ATPase directionality in isolated mouse liver mitochondria as a function of targeted inhibition of electron transfer pathways using various substrate-inhibitor combinations**. Traces are time courses of safranine O signal calibrated to $\Delta\Psi_{mt}$. **(A)** GM and increasing concentrations of Pro always contained in the medium; black (a): 0 mM; red (b): 0.5 mM; green (c): 1 mM; orange (d): 2 mM. **(B)** GM and increasing concentrations of Pro added where indicated; black (a): 0 mM; red (b): 0.25 mM; green (c): 0.5 mM; orange (d): 2 mM; blue (e): 5 mM. **(C)** As in B, but in traces b-f 15 mM βOH is additionally present; black (a): 0 mM; red (b): 0 mM; green (c): 0.25 mM; orange (d): 0.5 mM; blue (e): 2 mM; magenta (f): 5 mM. **(D)** Black (a): GM; red (b): GM and 5 mM Pro; green (c): GM & 1 nM SF added @500 s; orange (d): GM & 1 nM SF added @500 s and 5 mM Pro; blue (e): GM & 2 nM SF added @500 s; magenta (f): GM & 2 nM SF added @500 s and 5 mM Pro; cyan (g): GM & 3 nM SF added @500 s; grey (h): GM & 3 nM SF added @500 s and 5 mM Pro; brown (i): GM & 4 nM SF added @500 s; dark green (j): GM & 4 nM SF added @500 s and 5 mM Pro; dark yellow (k): GM & 5 nM SF added @500 s; dark blue (l): GM & 5 nM SF added @500 s and 5 mM Pro. **(E)** Myxothiazol (Myx); black trace: GM; red trace: GM and 5 mM Pro. **(F)** NaCN (CN); black (a): GM; red (b): GM and 0.5 mM Pro; green (c): GM and 1 mM Pro; orange (d): GM and 2 mM Pro. **(G)** Black (a): GM; red (b): GM and 5 mM Pro; green (c): GM and 2 mM THFA and 5 mM Pro; orange (d): GM and 5 mM THFA and 5 mM Pro; blue (e): GM and 10 mM THFA and 5 mM Pro; magenta (f): GM and 2 mM THFA; cyan (g): GM and 5 mM THFA; grey (h): GM and 10 mM THFA.
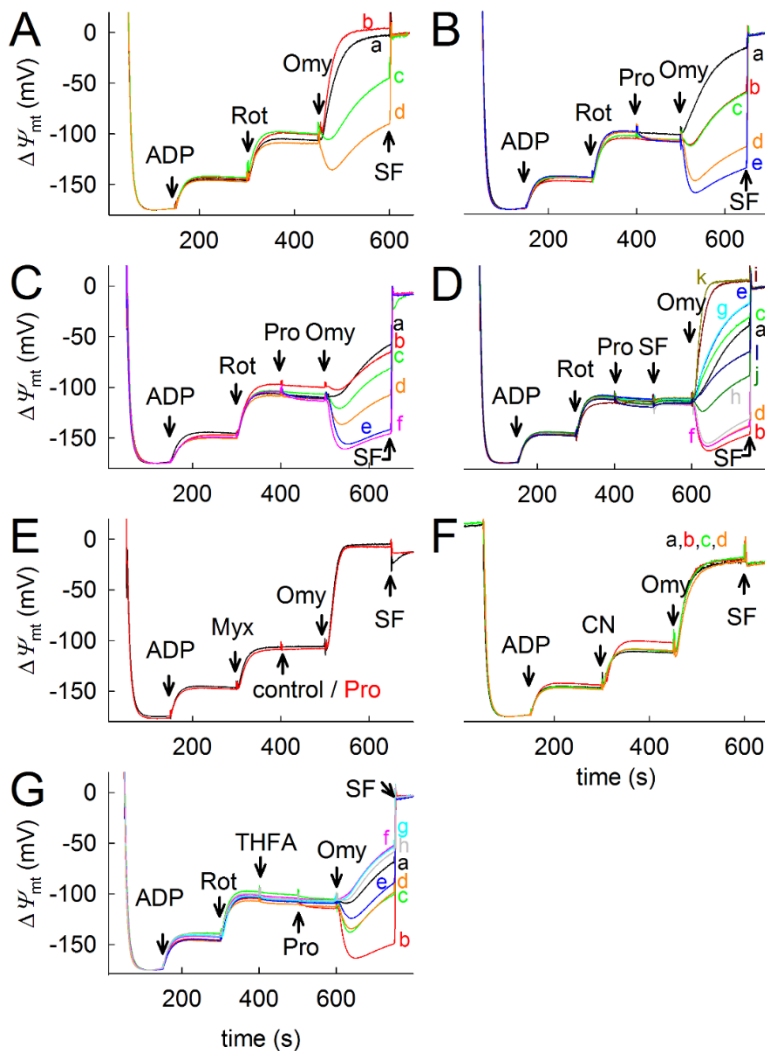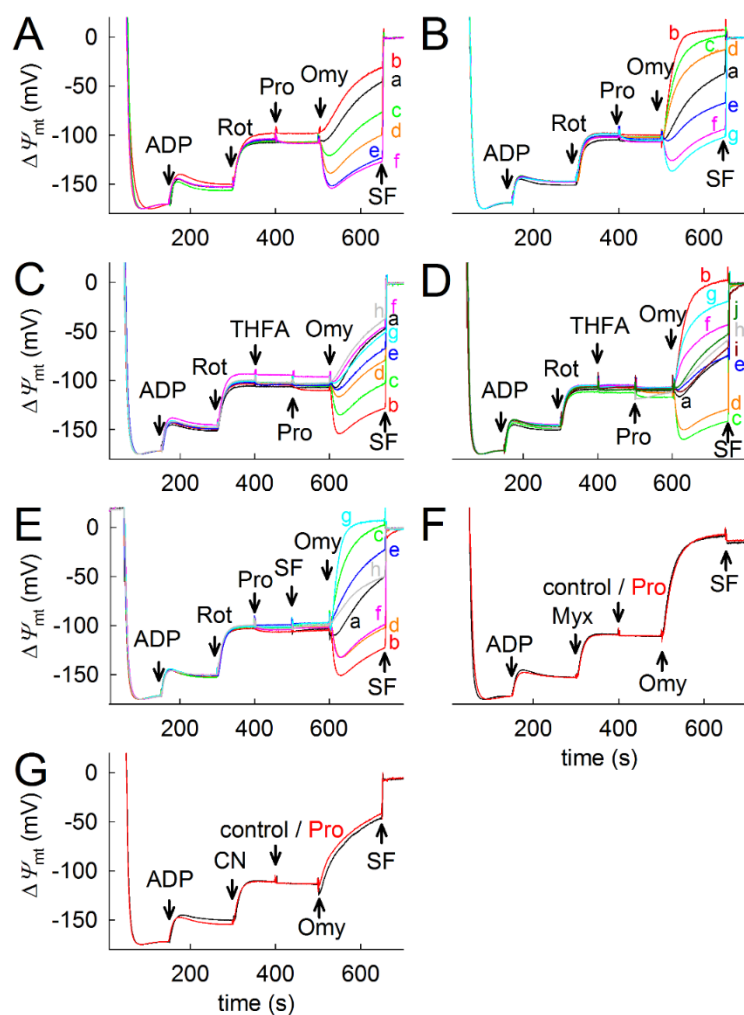
**Figure 25. The effect of proline on $F_1F_0$-ATPase directionality in isolated mouse kidney mitochondria as a function of targeted inhibition of electron transfer pathways using various substrate-inhibitor combinations**. Traces are time courses of safranine O signal calibrated to $\Delta\Psi_{mt}$. **(A)** GM and increasing concentrations of Pro; black (a): 0 mM; red (b): 0.25 mM; green (c): 0.5 mM; orange (d): 2 mM; blue (e): 5 mM; magenta (f): 10 mM. **(B)** GM (trace a) or GM & 5 mM itaconate (trace b to g), and increasing concentrations of Pro; black (a): 0 mM; red (b): 0 mM; green (c): 0.25 mM; orange (d): 0.5 mM; blue (e): 2 mM; magenta (f): 5 mM; cyan (g): 10 mM. **(C)** Black (a): GM; red (b): GM and 10 mM Pro; green (c): GM and 10 mM Pro and 2 mM THFA; orange (d): GM and 10 mM Pro and 5 mM THFA; blue (e): GM and 10 mM Pro and 10 mM THFA; magenta (f): GM and 2 mM THFA; cyan (g): GM and 5 mM THFA; grey (h): GM and 10 mM THFA. Traces are representative of at least 3 independent experiments. **(D)** Black (a): GM; red (b): GM & 5 mM itaconate; green (c): GM and 10 mM Pro; orange (d): GM & 5 mM itaconate and 10 mM Pro; blue (e): GM & 5 mM itaconate and 10 mM Pro and 2 mM THFA; magenta (f): GM & 5 mM itaconate and 10 mM Pro and 5 mM THFA; cyan (g): GM & 5 mM itaconate and 10 mM Pro and 10 mM THFA; grey (h): GM and 2 mM THFA; brown (i): GM and 5 mM THFA; dark green (j): GM and 10 mM THFA. **(E)** Black (a): GM; red (b): GM and 5 mM Pro; green (c): GM & 1 nM SF added @500 s; orange (d): GM & 1 nM SF added @500 s and 5 mM Pro; blue (e): GM & 2 nM SF added @500 s; magenta (f): GM & 2 nM SF added @500 s and 5 mM Pro; cyan (g): GM & 3 nM SF added @500 s; grey (h): GM & 3 nM SF added @500 s and 5 mM Pro. **(F)** myxothiazol (Myx); black trace: GM; red trace: GM and 10 mM Pro. **(G)** NaCN (CN); black trace: GM; red trace: GM and 10 mM proline.

Finally, proline exerted an effect on oligomycin-induced Q reduction in the presence of glutamate and malate (Figure 26B) just like in lieu of CAT (Figure 20B). These recordings were simultaneously made with oxygen consumption rate and rhodamine 123

fluorescence (indicative of $\Delta\Psi_{mt}$) (Figure panels 26A and 26C, respectively) using the NextGen-O2k. The reason(s) of the oligomycin-induced changes in Q redox state during CI inhibition as a function of proline were not investigated further.
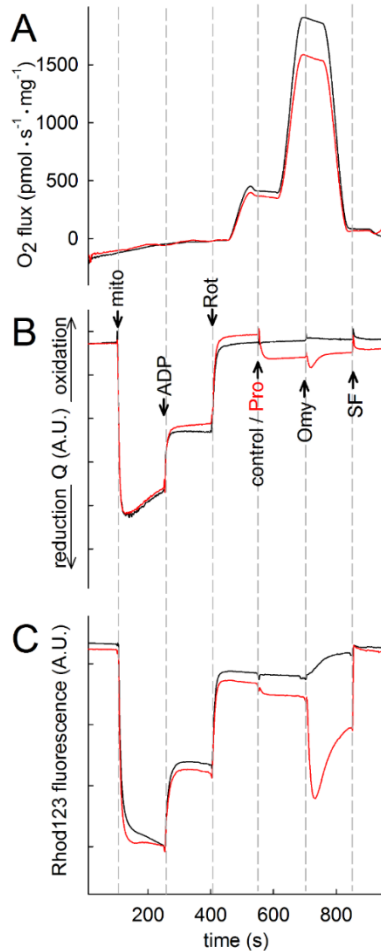


**Figure 26. The effect of proline on oligomycin-induced changes in Q redox state**. Time courses of oxygen consumption, Q redox state, and rhodamine 123 fluorescence indicative of $\Delta\Psi_{mt}$ (arbitrary units A.U.), respectively, recorded simultaneously from the same liver mitochondria using the NextGen-O2k and aligned on the dashed grey lines. 0.25 μM SF. Black trace: GM; red trace: GM and 5 mM Pro.

## 2.9. Fueling Complex III with duroquinone only partially mimics the benefits of proline

As shown from the results above, proline is oxidized by ProDH reducing Q which is in turn oxidized by CIII, also requiring CIV and oxygen as a final electron acceptor. Thus, we sought to compare the effects of proline with duroquinone (DQ), an artificial substrate of CIII. As shown in Figure panels 27A (for liver) and 27B (for kidney), DQ could partially mimic the effect of proline in maintaining $F_1F_0$-ATPase in forward mode. Higher concentrations of DQ had deleterious effects as they probably damage the mitochondrial inner membrane. Thus, proline is a far superior substrate for fueling CIII, though indirectly through Q. Furthermore, the effects of proline could not be reproduced by ornithine (Figure panel 27C), a metabolite forming GSA by transamination with Og (see Figure 1); mindful that GSA is downstream to proline oxidation by ProDH, it is concluded that proline effects are exclusively due to upstream Q reduction. In addition, proline could

also partially rescue ANT and $F_1F_0$-ATPase operation reversal induced by arsenite (NaAsO₂) -an inhibitor of dehydrogenases including oxoglutarate dehydrogenase (Figure 27D), thus its effects are unrelated to the dehydrogenase. Finally, the effects of proline were unaffected by dicoumarol, thus they are not mediated through diaphorases (Figure panel 27E).
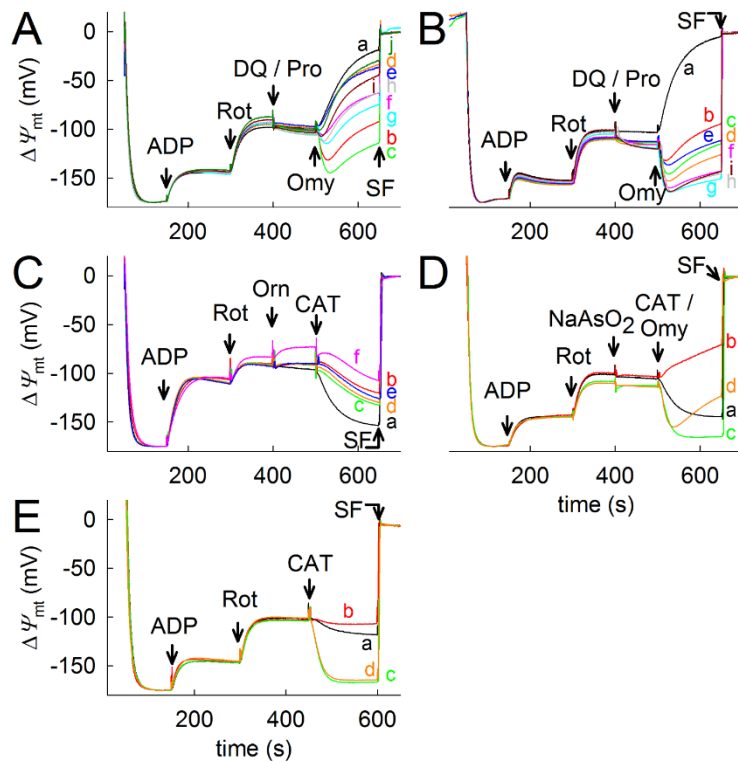


**Figure 27. Fuelling of CIII with duroquinone (DQ) but not ornithine partially mimics the effects of proline; neither arsenite nor dicoumarol antagonize proline**. Traces are time courses of safranine O signal calibrated to $\Delta\Psi_{mt}$. 0.25 μM SF. **(A)** Liver mitochondria; GM always present and the following additions; black (a): no other additions; red (b): 2 mM Pro; green (c): 5 mM Pro; orange (d): 0.01 mM duroquinone (DQ); blue (e): 0.05 mM DQ; magenta (f): 0.1 mM DQ; cyan (g): 0.2 mM DQ; grey (h): 0.3 mM DQ; brown (i): 0.4 mM DQ; dark green (j): 0.5 mM DQ. **(B)** kidney mitochondria; GM always present and the following additions; black (a): no other additions; red (b): 2 mM Pro; green (c): 5 mM Pro; orange (d): 10 mM Pro; blue (e): 0.01 mM DQ; magenta (f): 0.05 mM DQ; cyan (g): 0.1 mM DQ; grey (h): 0.2 mM DQ; brown (i): 0.3 mM DQ. **(C)** Liver mitochondria; 5 mM oxoglutarate (Og) always present and the following additions; black (a): no other additions; red (b): 2 mM ornithine (Orn); green (c): 5 mM Orn; orange (d): 10 mM Orn; blue (e): 20 mM Orn; magenta (f): 40 mM Orn. **(D)** Liver mitochondria; GM always present and the following additions; black (a): no other additions; red (b): 2 mM NaAsO₂; green (c): 5 mM Pro and 2 mM NaAsO₂; orange (d): 5 mM Pro and 2 mM NaASO₂. **(E)** Liver mitochondria. GM & 5 mM βOH always present and the following additions;.black (a): no other additions; red (b): 0.5 μM dicoumarol; green (c): 5 mM proline; orange (d): 5 mM proline & 0.5 μM dicoumarol.

## 3. Discussion

It is a textbook definition that when CI is inhibited and only NADH-linked substrates are available [29], $F_1F_0$-ATPase reverses, pumping protons out of the matrix even at the

cost of ATP consumption, preserving mitochondrial membrane potential [38], [39]. The most important conclusion of the present study is that the above statement does not apply when mitochondria oxidize proline through ProDH: here we showed that in CI-inhibited mitochondria exhibiting a sufficiently high ProDH activity, reduction of ubiquinone fueling CIII and CIV leading to proton pumping supports $\Delta\Psi_{mt}$ to a level at which the $F_1F_0$-ATPase maintains ATP production. This finding agrees with a modelling study in which the authors claimed that CI deficiency maybe compensated by proline oxidation [42].

Notably, this property of proline is not due to catabolism towards glutamate and oxoglutarate, as further catabolism of either metabolite requires CI activity. It is genuinely due to metabolism of proline through ProDH leading to Q reduction, fueling CIII. Relevant to this, duroquinone (DQ) could partially mimic the effects of proline fueling directly CIII but not to the same effect, as DQ is expected to exert undesirable effects such as ROS formation [43]. Several electron transfer pathways converge at the Q-junction, particularly the NADH- and succinate-linked (CI- and CII-linked) pathways and including the glycerophosphate pathway and fatty acid oxidation pathway with electron entry through the electron-transferring flavoprotein Complex into Q [51]. The proline pathway through ProDH is to be added to the list of ET pathways converging at the Q-junction with potential additive effects on OXPHOS and ET capacities when operating in combination.

S was the dominant $\alpha$-pathway with $J_S > J_{Pro}$. Then flux control ratios are $\alpha = J_S/J_{SPro}$ and $\beta = J_{Pro}/J_{SPro}$. Additivity $A_{\widetilde{\alpha\beta}}$ is defined as $(1 - \alpha)/\beta$ [29]. Complete additivity ($A_{\widetilde{\alpha\beta}} = 1$) is obtained when the linear sum of the component S- and Pro-pathway flux ($J_S + J_{Pro}$) equals the flux of the convergent SPro-pathway with the SPro-substrate combination ($J_{SPro}$). In the OXPHOS state, $A_{\widetilde{\alpha\beta}}$ was 2 in liver and 1.6 to 2.1 in kidney, indicating excess additivity and synergistic activation of $O_2$ flux. This contrasts with incomplete additivity of convergent NADH- and succinate-linked pathway flux [29]. LEAK respiration, however, is not linearly responsive to ET capacity, as reflected by the lower additivity observed in liver mitochondria. Surprisingly, additivity of LEAK respiration was negative in kidney mitochondria, which implies suppression of LEAK respiration by proline and consequently an over-proportional effect on coupling efficiency.

In conclusion, the ability of proline to maintain ATP production by the $F_1F_0$-ATPase in the presence of CI impairment should be added to an already long list involving this amino acid in cellular bioenergetics, osmoregulation, stress protection, apoptosis and cancer cell metabolism, reviewed in  [5] and [44].

## 4. Materials and methods

### 4.1. Animals

Mice were of mixed 129 Sv and C57Bl/6 background. The animals used in our study were of either sex and between 2 and 6 months of age. Data obtained from liver, kidney, brain or heart mitochondria of mice of a particular gender or age (2, 4 or 6 months) did not yield any qualitative differences, thus all data were pooled. Mice were housed in a room maintained at 20–22 °C on a 12-h light–dark cycle with food and water available ad

libitum. All experiments were approved by the Animal Care and Use Committee of the Semmelweis University (Egyetemi Állatkísérleti Bizottság).

## 4.2. Isolation of mitochondria

Liver, kidney, brain and heart mitochondria were isolated from mice as described in [45] and [36]. Protein concentration was determined using the bicinchoninic acid assay, and calibrated using bovine serum standards [46] using a Tecan Infinite® 200 PRO series plate reader (Tecan Deutschland GmbH, Crailsheim, Germany).

## 4.3. Determination of membrane potential (Δ𝛹mt) in isolated mitochondria

$\Delta\Psi_{mt}$ of isolated mitochondria (0.5 or 1 mg of mouse liver or kidney mitochondria in two ml buffer medium for normoxic or anoxic experiments, respectively; 0.25 or 0.5 mg of brain mitochondria per two ml of medium (the composition of which is described in [32]); 0.25 mg of mouse heart mitochondria per two ml of medium) was estimated fluorimetrically with safranine O [47] or rhodamine 123 [48] and expressed as arbitrary units or calibrated to millivolts as described in [32], acknowledging the considerations elaborated in [49] and [50] regarding inhibition of respiration and unspecific binding of safranine. Fluorescence was recorded using a Hitachi F-7000 spectrofluorimeter (Hitachi High Technologies, Maidenhead, UK) at a 5-Hz acquisition rate, at 495 nm and 585 nm excitation and emission wavelengths, respectively, or the Oroboros O2k (Oroboros Instruments, Innsbruck, Austria) equipped with the O2k-Fluo LED2-Module, or the NextGen-O2k prototype equipped with the O2k-Fluo Smart Module, with optical sensors including a LED (465 nm; <505 nm short-pass excitation filter), a photodiode and specific optical filters (>560 nm long-pass emission filter) [51]. Experiments were performed at 37 °C.

## 4.4. Mitochondrial respiration

Oxygen consumption was performed polarographically using an Oxygraph-2k. 0.5 or 1 mg of mouse liver or kidney mitochondria in two ml of buffer medium for normoxic or anoxic experiments, respectively; 0.25 mg of brain mitochondria per two ml of medium. Mitochondria were suspended in 2 ml incubation medium, the composition of which was identical to that for $\Delta\Psi_{mt}$ determination. Experiments were performed at 37 °C. Oxygen concentration (µM) and oxygen flux (pmol·s$^{-1}$·mg$^{-1}$; negative time derivative of oxygen concentration, divided by mitochondrial mass per volume and corrected for instrumental background oxygen flux arising from oxygen consumption of the oxygen sensor and back-diffusion into the chamber) were recorded using DatLab software (Oroboros Instruments).

## 4.5. Determination of NADH autofluorescence in isolated mitochondria

NADH autofluorescence was measured using two different instruments: (1) Hitachi F-7000 fluorescence spectrophotometer, and (2) the NADH-Module of the NextGen-O2k (Oroboros Instruments). NADH measurements were performed in a Hitachi F-7000 fluorescence spectrophotometer at a 5 Hz acquisition rate, using 340 and 435 nm

excitation and emission wavelengths, respectively. The NextGen-O2k allows simultaneous measurement of oxygen consumption and NADH autofluorescence, incorporating an ultraviolet (UV) LED with an excitation wavelength of 365 nm and an integrated spectrometer which records a wavelength range between 450 and 590 nm. The light intensity of the LED was set to 10 mA. 0.5 mg of mouse liver, kidney, brain, 0.25 mg of mouse heart mitochondria were suspended in 2 ml incubation medium, the composition of which was identical to that for $\Delta\Psi_{mt}$ determination, as described in [32]. Experiments were performed at 37 °C.

## 4.6.  Mitochondrial Q redox state

Coenzyme Q redox state of isolated mitochondria suspended in a buffer composition as described in [32] was followed amperometically using a three electrode system with coenzyme Q$_2$ (CoQ$_2$, 1 µM) as mediator, using the Q-Module of the NextGen-O2k [52]. The reference electrode was Ag/AgCl/(3M KCl). The auxiliary electrode was made of platinum and the working electrode was fabricated from glassy carbon. Oxidation peak potential of CoQ$_2$ measured by cyclic voltammetry was set to the glassy carbon to measure the oxidation of reduced CoQ$_2$. Q redox state was recorded simultaneously with O$_2$ flux and rhodamine 123 fluorescence.

## 4.7.  Determination of proline dehydrogenase activity

ProDH activity was determined in alamethicin-treated mitochondria immediately after isolation, as described in [53], with minor modifications. Briefly, reaction was carried out in a 50 mM phosphate buffer (pH 7.4) with 0.25 mg mitochondria, 10 µg alamethicin, 1 µM cytochrome c and proline concentrations indicated in legends. After 30 minutes at 25°C while shaking (500 rpm), the reaction was stopped by the addition of half the final volume 10 w/v % trichloroacetic acid and one-tenth the final volume of freshly made 0.1 M 2-aminobenzaldehyde dissolved in 40 v/v % ethanol. After 30 minutes, the absorbance on 440 nm was read against a parallel blank without substrate. Concentration of P5C was calculated using $\varepsilon=2.58$ mM$^{-1}\cdot$cm$^{-1}$ [54].

## 4.8.  Reagents

Standard laboratory chemicals, duroquinone, tetrahydro-2-furoic acid and S-5-oxo-2-tetrahydrofurancarboxylic acid were from Sigma Aldrich (St Louis, Missouri, US). SF6847 and atpenin A5 were purchased from Enzo Life Sciences (ELS AG, Lausen, Switzerland). Mitochondrial substrates were dissolved in bi-distilled water and titrated to pH 7.0 with KOH. ADP was purchased as a K$^+$ salt of the highest purity available (Merck) and titrated to pH 6.9.

Concentrations of glutamate (G), malate (M), and oxoglutarate (Og) were always 5 mM when present. Succinate was added where indicated (S, 5 mM). ADP concentrations were 2 mM where titrations are indicated. Rotenone (Rot, 1 µM), myxothiazol (Myx, 1 µM; or 0.1 µM when specified), carboxyatractyloside (CAT, 1 µM), oligomycin (Omy, 10 µM), NaCN (CN, 1 mM), SF6847 (SF, 1 µM; or 0.25 µM when specified).

## 4.9.  Figures on time courses

All traces are representative of at least 3 independent experiments. At the end of many experiments, the uncoupler SF6847 (SF) was added to confer a complete collapse of $\Delta\Psi_{mt}$ as a point of reference.

## Abbreviations

| | | | |
|---|---|---|---|
| ALDH4A1 | delta-1-pyrroline-5-carboxylate dehydrogenase | M | malate |
| ANT | adenine nucleotide translocase | mtIM | mitochondrial inner membrane |
| ASAT | aspartate aminotransferase | Myx | myxothiazol |
| βOH | β-hydroxybutyrate | OAT | ornithine aminotransferase |
| CAT | carboxyatractyloside | Og | 2-oxoglutarate (α-ketoglutarate) |
| CI, CII, CIII, CIV | respiratory Complexes I to IV | | |
| CN | cyanide (NaCN) | OgDH | oxoglutarate dehydrogenase |
| DQ | duroquinone | Omy | oligomycin |
| ET | electron transfer | OXPHOS capacity | respiration at kinetically saturating [ADP] |
| ETS | electron transfer system | | |
| $\Delta\Psi_{mt}$ | mitochondrial membrane potential | Pro | proline |
| G | glutamate | ProDH | proline dehydrogenase |
| GDH | glutamate dehydrogenase | P5C | pyrroline-5-carboxylate |
| GM | glutamate & malate | Q | mitochondrial ETS-reactive coenzyme Q |
| GSA | glutamate semi-aldehyde | | |
| Itac | itaconate | Rot | rotenone |
| THFA | tetrahydro-2-furoic acid | Rox | residual oxygen consumption |
| LEAK respiration | resting respiration in the absence of ADP | S | succinate |
| | | SCS | succinate-CoA ligase (succinyl-CoA synthetase) |
| | | SF | uncoupler SF6847 |

## References

1. Taggart, J.V.; Krakaur, R.B. Studies on the cyclophorase system; the oxidation of proline and hydroxyproline. *J Biol Chem* **1949**, *177*, 641-653.
2. Johnson, A.B.; Strecker, H.J. The interconversion of glutamic acid and proline. IV. The oxidation of proline by rat liver mitochondria. *J Biol Chem* **1962**, *237*, 1876-1882.
3. McKnight, J.A.; Hird, F.J. The oxidation of proline by mitochondrial preparations. *Comp Biochem Physiol B* **1986**, *85*, 289-294, doi:10.1016/0305-0491(86)90002-7.
4. Scaraffia, P.Y.; Wells, M.A. Proline can be utilized as an energy substrate during flight of Aedes aegypti females. *J Insect Physiol* **2003**, *49*, 591-601, doi:10.1016/s0022-1910(03)00031-3.
5. McDonald, A.E.; Pichaud, N.; Darveau, C.A. "Alternative" fuels contributing to mitochondrial electron transport: Importance of non-classical pathways in the diversity of animal metabolism. *Comp Biochem Physiol B Biochem Mol Biol* **2018**, *224*, 185-194, doi:10.1016/j.cbpb.2017.11.006.
6. Gade, G.; Auerswald, L. Beetles' choice--proline for energy output: control by AKHs. *Comp Biochem Physiol B Biochem Mol Biol* **2002**, *132*, 117-129, doi:10.1016/s1096-4959(01)00541-3.
7. D'Aniello, C.; Patriarca, E.J.; Phang, J.M.; Minchiotti, G. Proline Metabolism in Tumor Growth and Metastatic Progression. *Front Oncol* **2020**, *10*, 776, doi:10.3389/fonc.2020.00776.

8.  Phang, J.M. Proline Metabolism in Cell Regulation and Cancer Biology: Recent Advances and Hypotheses. *Antioxid Redox Signal* **2019**, *30*, 635-649, doi:10.1089/ars.2017.7350.
9.  Hancock, C.N.; Liu, W.; Alvord, W.G.; Phang, J.M. Co-regulation of mitochondrial respiration by proline dehydrogenase/oxidase and succinate. *Amino Acids* **2016**, *48*, 859-872, doi:10.1007/s00726-015-2134-7.
10. Vettore, L.A.; Westbrook, R.L.; Tennant, D.A. Proline metabolism and redox; maintaining a balance in health and disease. *Amino Acids* **2021**, doi:10.1007/s00726-021-03051-2.
11. Adams, E.; Frank, L. Metabolism of proline and the hydroxyprolines. *Annu Rev Biochem* **1980**, *49*, 1005-1061, doi:10.1146/annurev.bi.49.070180.005041.
12. Du, J.; Zhu, S.; Lim, R.R.; Chao, J.R. Proline metabolism and transport in retinal health and disease. *Amino Acids* **2021**, doi:10.1007/s00726-021-02981-1.
13. Meyer, J. Proline transport in rat liver mitochondria. *Arch Biochem Biophys* **1977**, *178*, 387-395, doi:10.1016/0003-9861(77)90208-9.
14. Atlante, A.; Passarella, S.; Pierro, P.; Quagliariello, E. Proline transport in rat kidney mitochondria. *Arch Biochem Biophys* **1994**, *309*, 139-148, doi:10.1006/abbi.1994.1096.
15. Summitt, C.B.; Johnson, L.C.; Jonsson, T.J.; Parsonage, D.; Holmes, R.P.; Lowther, W.T. Proline dehydrogenase 2 (PRODH2) is a hydroxyproline dehydrogenase (HYPDH) and molecular target for treating primary hyperoxaluria. *Biochem J* **2015**, *466*, 273-281, doi:10.1042/BJ20141159.
16. Pandhare, J.; Donald, S.P.; Cooper, S.K.; Phang, J.M. Regulation and function of proline oxidase under nutrient stress. *J Cell Biochem* **2009**, *107*, 759-768, doi:10.1002/jcb.22174.
17. Erecinska, M. Ubiquinone in proline oxidation. *Arch Int Pharmacodyn Ther* **1965**, *158*, 209-215.
18. Chinopoulos, C. The "B space" of mitochondrial phosphorylation. *J Neurosci Res* **2011**, *89*, 1897-1904, doi:10.1002/jnr.22659.
19. Kowaloff, E.M.; Granger, A.S.; Phang, J.M. Alterations in proline metabolic enzymes with mammalian development. *Metabolism* **1976**, *25*, 1087-1094, doi:10.1016/0026-0495(76)90016-0.
20. Schmidt, J.A.; Rinaldi, S.; Scalbert, A.; Ferrari, P.; Achaintre, D.; Gunter, M.J.; Appleby, P.N.; Key, T.J.; Travis, R.C. Plasma concentrations and intakes of amino acids in male meat-eaters, fish-eaters, vegetarians and vegans: a cross-sectional analysis in the EPIC-Oxford cohort. *Eur J Clin Nutr* **2016**, *70*, 306-312, doi:10.1038/ejcn.2015.144.
21. Mc, M.R.; Lund, C.C.; Oncley, J.L. Unbound amino acid concentrations in human blood plasmas. *J Clin Invest* **1957**, *36*, 1672-1679, doi:10.1172/JCI103568.
22. Frame, E.G. The levels of individual free amino acids in the plasma of normal man at various intervals after a high-protein meal. *J Clin Invest* **1958**, *37*, 1710-1723, doi:10.1172/JCI103763.
23. Martinez, M.; Frank, A.; Diez-Tejedor, E.; Hernanz, A. Amino acid concentrations in cerebrospinal fluid and serum in Alzheimer's disease and vascular dementia. *J Neural Transm Park Dis Dement Sect* **1993**, *6*, 1-9, doi:10.1007/BF02252617.
24. Liu, Z.; Jeppesen, P.B.; Gregersen, S.; Bach Larsen, L.; Hermansen, K. Chronic Exposure to Proline Causes Aminoacidotoxicity and Impaired Beta-Cell Function: Studies In Vitro. *Rev Diabet Stud* **2016**, *13*, 66-78, doi:10.1900/RDS.2016.13.66.
25. Newton, H.; Wang, Y.F.; Camplese, L.; Mokochinski, J.B.; Kramer, H.B.; Brown, A.E.X.; Fets, L.; Hirabayashi, S. Systemic muscle wasting and coordinated tumour response drive tumourigenesis. *Nat Commun* **2020**, *11*, 4653, doi:10.1038/s41467-020-18502-9.
26. Scharff, R.; Wool, I.G. Effect of diabetes on the concentration of amino acids in plasma and heart muscle of rats. *Biochem J* **1966**, *99*, 173-178, doi:10.1042/bj0990173.
27. Gnaiger, E. et al — MitoEAGLE Task Group. Mitochondrial physiology. *Bioenerg Commun* **2020**, *1*, 1-44, doi:10.26124/bec:2020-0001.v1.
28. Nemeth, B.; Doczi, J.; Csete, D.; Kacso, G.; Ravasz, D.; Adams, D.; Kiss, G.; Nagy, A.M.; Horvath, G.; Tretter, L.; et al. Abolition of mitochondrial substrate-level phosphorylation by itaconic acid produced by LPS-induced Irg1 expression in cells of murine macrophage lineage. *FASEB J* **2016**, *30*, 286-300, doi:10.1096/fj.15-279398.
29. Gnaiger, E. Mitochondrial pathways and respiratory control. An introduction to OXPHOS analysis 5th ed. *Bioenerg Commun* **2020**, *2*, 112 pp, doi:10.26124/bec:2020-0002.
30. Luo, M.; Arentson, B.W.; Srivastava, D.; Becker, D.F.; Tanner, J.J. Crystal structures and kinetics of monofunctional proline dehydrogenase provide insight into substrate recognition and conformational

changes associated with flavin reduction and product release. *Biochemistry* **2012**, *51*, 10099-10108, doi:10.1021/bi301312f.

31. Scott, G.K.; Yau, C.; Becker, B.C.; Khateeb, S.; Mahoney, S.; Jensen, M.B.; Hann, B.; Cowen, B.J.; Pegan, S.D.; Benz, C.C. Targeting Mitochondrial Proline Dehydrogenase with a Suicide Inhibitor to Exploit Synthetic Lethal Interactions with p53 Upregulation and Glutaminase Inhibition. *Mol Cancer Ther* **2019**, *18*, 1374-1385, doi:10.1158/1535-7163.MCT-18-1323.

32. Chinopoulos, C.; Gerencser, A.A.; Mandi, M.; Mathe, K.; Torocsik, B.; Doczi, J.; Turiak, L.; Kiss, G.; Konrad, C.; Vajda, S.; et al. Forward operation of adenine nucleotide translocase during F0F1-ATPase reversal: critical role of matrix substrate-level phosphorylation. *FASEB J* **2010**, *24*, 2405-2416, doi:10.1096/fj.09-149898.

33. Chinopoulos, C. Mitochondrial consumption of cytosolic ATP: not so fast. *FEBS Lett* **2011**, *585*, 1255-1259, doi:10.1016/j.febslet.2011.04.004.

34. Klingenberg, M. The ADP and ATP transport in mitochondria and its carrier. *Biochim Biophys Acta* **2008**, *1778*, 1978-2021, doi:10.1016/j.bbamem.2008.04.011.

35. Alexandre, A.; Reynafarje, B.; Lehninger, A.L. Stoichiometry of vectorial H+ movements coupled to electron transport and to ATP synthesis in mitochondria. *Proc Natl Acad Sci U S A* **1978**, *75*, 5296-5300, doi:10.1073/pnas.75.11.5296.

36. Kiss, G.; Konrad, C.; Doczi, J.; Starkov, A.A.; Kawamata, H.; Manfredi, G.; Zhang, S.F.; Gibson, G.E.; Beal, M.F.; Adam-Vizi, V.; et al. The negative impact of alpha-ketoglutarate dehydrogenase complex deficiency on matrix substrate-level phosphorylation. *FASEB J* **2013**, *27*, 2392-2406, doi:10.1096/fj.12-220202.

37. Bui, D.; Ravasz, D.; Chinopoulos, C. The Effect of 2-Ketobutyrate on Mitochondrial Substrate-Level Phosphorylation. *Neurochem Res* **2019**, *44*, 2301-2306, doi:10.1007/s11064-019-02759-8.

38. Chinopoulos, C.; Tretter, L.; Adam-Vizi, V. Depolarization of in situ mitochondria due to hydrogen peroxide-induced oxidative stress in nerve terminals: inhibition of alpha-ketoglutarate dehydrogenase. *J Neurochem* **1999**, *73*, 220-228, doi:10.1046/j.1471-4159.1999.0730220.x.

39. Martinez-Reyes, I.; Diebold, L.P.; Kong, H.; Schieber, M.; Huang, H.; Hensley, C.T.; Mehta, M.M.; Wang, T.; Santos, J.H.; Woychik, R.; et al. TCA Cycle and Mitochondrial Membrane Potential Are Necessary for Diverse Biological Functions. *Mol Cell* **2016**, *61*, 199-209, doi:10.1016/j.molcel.2015.12.002.

40. Vafai, S.B.; Mevers, E.; Higgins, K.W.; Fomina, Y.; Zhang, J.; Mandinova, A.; Newman, D.; Shaw, S.Y.; Clardy, J.; Mootha, V.K. Natural Product Screening Reveals Naphthoquinone Complex I Bypass Factors. *PLoS One* **2016**, *11*, e0162686, doi:10.1371/journal.pone.0162686.

41. Ravasz, D.; Kacso, G.; Fodor, V.; Horvath, K.; Adam-Vizi, V.; Chinopoulos, C. Reduction of 2-methoxy-1,4-naphtoquinone by mitochondrially-localized Nqo1 yielding NAD(+) supports substrate-level phosphorylation during respiratory inhibition. *Biochim Biophys Acta Bioenerg* **2018**, *1859*, 909-924, doi:10.1016/j.bbabio.2018.05.002.

42. Zielinski, L.P.; Smith, A.C.; Smith, A.G.; Robinson, A.J. Metabolic flexibility of mitochondrial respiratory chain disorders predicted by computer modelling. *Mitochondrion* **2016**, *31*, 45-55, doi:10.1016/j.mito.2016.09.003.

43. Fato, R.; Bergamini, C.; Leoni, S.; Lenaz, G. Mitochondrial production of reactive oxygen species: role of complex I and quinone analogues. *Biofactors* **2008**, *32*, 31-39, doi:10.1002/biof.5520320105.

44. Tanner, J.J.; Fendt, S.M.; Becker, D.F. The Proline Cycle As a Potential Cancer Therapy Target. *Biochemistry* **2018**, *57*, 3433-3444, doi:10.1021/acs.biochem.8b00215.

45. Chinopoulos, C.; Vajda, S.; Csanady, L.; Mandi, M.; Mathe, K.; Adam-Vizi, V. A novel kinetic assay of mitochondrial ATP-ADP exchange rate mediated by the ANT. *Biophys J* **2009**, *96*, 2490-2504, doi:10.1016/j.bpj.2008.12.3915.

46. Smith, P.K.; Krohn, R.I.; Hermanson, G.T.; Mallia, A.K.; Gartner, F.H.; Provenzano, M.D.; Fujimoto, E.K.; Goeke, N.M.; Olson, B.J.; Klenk, D.C. Measurement of protein using bicinchoninic acid. *Anal Biochem* **1985**, *150*, 76-85, doi:10.1016/0003-2697(85)90442-7.

47. Akerman, K.E.; Wikstrom, M.K. Safranine as a probe of the mitochondrial membrane potential. *FEBS Lett* **1976**, *68*, 191-197, doi:10.1016/0014-5793(76)80434-6.

48. Emaus, R.K.; Grunwald, R.; Lemasters, J.J. Rhodamine 123 as a probe of transmembrane potential in isolated rat-liver mitochondria: spectral and metabolic properties. *Biochim Biophys Acta* **1986**, *850*, 436-448, doi:10.1016/0005-2728(86)90112-x.

49. Valle, V.G.; Pereira-da-Silva, L.; Vercesi, A.E. Undesirable feature of safranine as a probe for mitochondrial membrane potential. *Biochem Biophys Res Commun* **1986**, *135*, 189-195, doi:10.1016/0006-291x(86)90961-7.
50. Chinopoulos, C.; Adam-Vizi, V. Mitochondrial Ca2+ sequestration and precipitation revisited. *FEBS J* **2010**, *277*, 3637-3651, doi:10.1111/j.1742-4658.2010.07755.x.
51. Krumschnabel, G.; Eigentler, A.; Fasching, M.; Gnaiger, E. Use of safranin for the assessment of mitochondrial membrane potential by high-resolution respirometry and fluorometry. *Methods Enzymol* **2014**, *542*, 163-181, doi:10.1016/B978-0-12-416618-9.00009-1.
52. Komlódi T, C.L., Doerrier C, Moore AL, Rich PR, Gnaiger E. Coupling and pathway control of coenzyme Q redox state and respiration in isolated mitochondria. *Bioenerg Commun* **2021**, doi: 10.26124/bec:2021-0003.
53. Kawabata, Y.; Katunuma, N.; Sanada, Y. Characteristics of proline oxidase in rat tissues. *J Biochem* **1980**, *88*, 281-283.
54. Mezl, V.A.; Knox, W.E. Properties and analysis of a stable derivative of pyrroline-5-carboxylic acid for use in metabolic studies. *Anal Biochem* **1976**, *74*, 430-440, doi:10.1016/0003-2697(76)90223-2.

## Supplement

### Table S1. Additivity of OXPHOS capacity or LEAK respiration of the convergent Proline- and Succinate-pathways. Analysis of unpaired tests, summarized in Table 1. For definition of additivity and equations 7.1 and 7.2, see [S1].

**Liver Fig 3D** (pmol·s$^{-1}$·mg$^{-1}$)

| | Pro: 2 mM LEAK | Pro: 2 mM OXPHOS | S: 5 mM LEAK | S: 5 mM OXPHOS | SPro: 5 mM S + 2 mM Pro LEAK | SPro: 5 mM S + 2 mM Pro OXPHOS | | S+Pro | SPro/(S+Pro) Eq. 7.1 β | Pro/SPro Eq. 7.1 α | S/SPro | Additivity Eq: 7.2 |
|---|---|---|---|---|---|---|---|---|---|---|---|---|
| | 217 | 811 | 336 | 1072 | 645 | 3070 | | | | | | |
| | 390 | 958 | 294 | 1219 | 448 | 2506 | | | | | | |
| | 195 | 870 | 345 | 1203 | 501 | 3041 | | | | | | |
| | 372 | 1090 | 336 | 1542 | 671 | 3387 | | | | | | |
| | 339 | 927 | | | 402 | 2023 | | | | | | |
| | 157 | 556 | | | | | | | | | | |
| median | | 898 | | 1211 | | 3041 | OXPHOS | 2109 | 1.44 | 0.30 | 0.40 | 2.04 |
| median | 278 | | 336 | | 501 | | LEAK | 614 | 0.82 | 0.55 | 0.67 | 0.59 |

**Liver Fig 3E** (pmol·s$^{-1}$·mg$^{-1}$)

| | Pro: 5 mM LEAK | Pro: 5 mM OXPHOS | S: 5 mM LEAK | S: 5 mM OXPHOS | SPro: 5 mM S + 5 mM Pro LEAK | SPro: 5 mM S + 5 mM Pro OXPHOS | | S+Pro | SPro/(S+Pro) Eq. 7.1 β | Pro/SPro Eq. 7.1 α | S/SPro | Additivity Eq: 7.2 |
|---|---|---|---|---|---|---|---|---|---|---|---|---|
| | 219 | 754 | 336 | 1072 | 565 | 2974 | | | | | | |
| | 204 | 897 | 294 | 1219 | 418 | 2441 | | | | | | |
| | 300 | 1406 | 345 | 1203 | 873 | 4969 | | | | | | |
| | 179 | 906 | 336 | 1542 | 607 | 3429 | | | | | | |
| | 200 | 900 | | | 369 | 1991 | | | | | | |
| | 223 | 886 | | | | | | | | | | |
| | 157 | 1052 | | | | | | | | | | |
| | 369 | 1170 | | | | | | | | | | |
| | 349 | 1218 | | | | | | | | | | |
| | 197 | 794 | | | | | | | | | | |
| | 228 | 819 | | | | | | | | | | |
| | 310 | 970 | | | | | | | | | | |
| | 373 | 1283 | | | | | | | | | | |
| median | | 906 | | 1211 | | 2974 | OXPHOS | 2117 | 1.41 | 0.30 | 0.41 | 1.95 |
| median | 223 | | 336 | | 565 | | LEAK | 559 | 1.01 | 0.40 | 0.59 | 1.03 |

**Kidney Fig 3I** (pmol·s$^{-1}$·mg$^{-1}$)

| | Pro: 2 mM LEAK | Pro: 2 mM OXPHOS | S: 5 mM LEAK | S: 5 mM OXPHOS | SPro: 5 mM S + 2 mM Pro LEAK | SPro: 5 mM S + 2 mM Pro OXPHOS | | S+Pro | SPro/(S+Pro) Eq. 7.1 β | Pro/SPro Eq. 7.1 α | S/SPro | Additivity Eq: 7.2 |
|---|---|---|---|---|---|---|---|---|---|---|---|---|
| | 119 | 809 | 1233 | 3435 | 946 | 4288 | | | | | | |
| | 233 | 717 | 991 | 2217 | 909 | 3475 | | | | | | |
| | 263 | 734 | 945 | 2367 | 851 | 4164 | | | | | | |
| | 214 | 641 | 787 | 1904 | 756 | 3007 | | | | | | |
| median | | 725 | | 2292 | | 3820 | OXPHOS | 3017 | 1.27 | 0.19 | 0.60 | 2.11 |
| median | 223 | | 968 | | 880 | | LEAK | 1191 | 0.74 | 0.25 | 1.10 | -0.39 |

**Kidney Fig 3J** (pmol·s$^{-1}$·mg$^{-1}$)

| | Pro: 5 mM LEAK | Pro: 5 mM OXPHOS | S: 5 mM LEAK | S: 5 mM OXPHOS | SPro: 5 mM S + 5 mM Pro LEAK | SPro: 5 mM S + 5 mM Pro OXPHOS | | S+Pro | SPro/(S+Pro) Eq. 7.1 β | Pro/SPro Eq. 7.1 α | S/SPro | Additivity Eq: 7.2 |
|---|---|---|---|---|---|---|---|---|---|---|---|---|
| | 188 | 1088 | 1233 | 3435 | 1120 | 5205 | | | | | | |
| | 377 | 987 | 991 | 2217 | 993 | 4072 | | | | | | |
| | 322 | 907 | 945 | 2367 | 802 | 3869 | | | | | | |
| | 302 | 729 | 787 | 1904 | 799 | 3793 | | | | | | |
| | 761 | 1884 | | | | | | | | | | |
| | 384 | 1094 | | | | | | | | | | |
| median | | 1038 | | 2292 | | 3971 | OXPHOS | 3330 | 1.19 | 0.26 | 0.58 | 1.62 |
| median | 349 | | 968 | | 898 | | LEAK | 1317 | 0.68 | 0.39 | 1.08 | -0.20 |

## References

S1. Gnaiger E (2020) Mitochondrial pathways and respiratory control. An introduction to OXPHOS analysis. 5th ed. Bioenerg Commun 2020.2:112 pp. https://doi.org/10.26124/bec:2020-0002